NTNU – Trondheim
Norwegian University of
Science and Technology

Optimization of Strength and Permeability of Tape casted Porous $La_{0.2}Sr_{0.8}Fe_{0.8}Ta_{0.2}O_{3-\delta}$

Petter Wibe

Materials Technology
Submission date: July 2012
Supervisor: Kjell Wiik, IMTE
Co-supervisor: Jonas Gurauskis, IMT
Ørjan Fossmark Lohne, IMT

Norwegian University of Science and Technology
Department of Materials Science and Engineering

Declaration

I declare that the work described in this Master's thesis has been performed independently and in accordance with the rules and regulations for examinations at the Norwegian University of Science and Technology, NTNU

Petter Wibe

Trondheim, July 6th, 2012

Abstract

Ceramics with mixed ionic and electronic conductivity are being investigated for oxygen separation from air, intended for the production of syngas. Asymmetric membranes, consisting of a dense membrane co-sintered with a porous support are expected to achieve a high flux of oxygen and at the same time adequate strength.

As the porous substrate is mainly intended for strength contribution, it is crucial that the flux of oxygen through the dense membrane is not limited by the flow of air through the porous substrate. An oxygen flux of 10 ml min^{-1} cm^{-2} should be achieved at operating temperatures (800-1000 °C) for the substrate to be commercially attractive. A biaxial strength of 34MPa has been obtained by similar porous substrates.

Four different strategies for achieving high permeating substrates made by solid state $La_{0.2}Sr_{0.8}Fe_{0.8}Ta_{0.2}O_{3-\delta}$ have been evaluated. Pressed porous substrates were produced both with and without the use of pore formers. The most promising compositions with respect to porosity and permeability were tape casted and characterized with respect to porosity, permeability and strength.

The most promising substrate was made by tape casting $La_{0.2}Sr_{0.8}Fe_{0.8}Ta_{0.2}O_{3-\delta}$ and carbon black. With 27 % apparent porosity, it achieved an air permeability of 3,5nPm at room temperature, an estimated flux of 115 ml min^{-1} cm^{-2} at 1000 °C and a biaxial strength of 37.4MPa.

Sammendrag

Keramer med både ionisk og elektronisk ledningsevne forskes på for å kunne brukes i oksygenseparasjon fra luft, tilsiktet produksjon av syntesegass. Asymmetriske membraner, bestående av en tett membran sintret sammen med et porøst substrat, forventes å kunne oppnå høy oksygenfluks og samtidig tilstrekkelig styrke.

Siden substratene først og fremst er ment som styrkebidrag er det viktig at oksygenfluksen gjennom den tette membranen ikke begrenses av luftstrømmen gjennom det porøse substratet. De porøse substratene burde derfor oppnå en oksygenfluks på 10 ml min^{-1} cm^{-2} ved driftstemperatur (800-1000 °C) for at de skal være kommersielt attraktive. En biaksial styrke på 34MPa har blitt oppnådd av lignende porøse substrater.

Fire forskjellige fremgangsmåter for å oppnå porøse substrater av $La_{0.2}Sr_{0.8}Fe_{0.8}Ta_{0.2}O_{3-\delta}$ med høy luftpermeabilitet har blitt evaluert. Porøse substrater ble produsert både med og uten bruk av poredannere. De substratene som virket mest lovende med hensyn til åpen porøsitet og permeabilitet, ble videre produsert ved båndstøping og karakterisert med hensyn til porøsitet, permeabilitet og styrke.

Det beste substratet ble produsert ved å båndstøpe $La_{0.2}Sr_{0.8}Fe_{0.8}Ta_{0.2}O_{3-\delta}$ og grafitt. Med en åpen porøsitet på 27 % oppnådde det en permeabilitet på 3,5nPm ved romtemperatur, en estimert fluks på 115 ml min^{-1} cm^{-2} ved 1000 °C og en biaksial styrke på 37,4MPa.

Preface

This master thesis was written at the Department of Materials Science and Engineering at the Norwegian University of Science and Technology during the spring of 2012.

I would like to thank my main supervisor Prof. Kjell Wiik for valuable guidance and directions during this thesis, and my co-supervisors Dr. Jonas Gurauskis and PhD-student Ørjan Fossmark Lohne for their practical advice and support in the experimental part of the work. Finally, I would like to thank the SINTEF-unit Materials and Chemistry at KII for sharing their thoughts, ideas and expert knowledge concerning the experimental part of this work.

Contents

List of abbreviations

BET	Brunauer-Emmett-Teller, surface area analysis
CA	Cellulose acetate
CB	Carbon black
DIL	Dilatometer
EtOH	Ethanol
LSFTa	$La_{0.2}Sr_{0.8}Fe_{0.8}Ta_{0.2}O_{3-\delta}$
MIEC	Mixed ionic-electronic conducting
R.T.	Room temperature
SEM	Scanning electron microscope
SA	Sintering aid
Sa	Surface area
SOEC	Solid oxide electrolysis cell
SOFC	Solid oxide fuel cell
Syngas	Synthesis gas, a mixture of CO and H_2 gas
TGA	Thermal gravimetric analysis
XRD	X-ray diffraction

List of symbols

A	surface area
a	effective contact radius of the ball, ball-on-ring test
b	radius of the supporting ring, ball-on-ring test
d	particle diameter
D_a	air permeability
D_S	self-diffusion coefficient
F	Faraday constant
F_N	applied force
h	thickness of the substrate
jO_2	oxygen flux
K	RDC-145 flow factor
k_S	surface exchange coefficient
Mw_x	molar weight of species x
m_1	dry weight of substrate
m_2	weight of substrate immersed in liquid
m_3	weight of substrate in air, with immersed liquid in pores
ΔP	pressure drop across the substrate
pO_2	oxygen partial pressure
R	specimen radius
T	temperature
t_e	electronic transference number
t_i	transference number of species i
V	volume
υ	Poisson’s ratio

Greek

$\dot{\gamma}$	shear rate
η	viscosity
η_a	viscosity of air
μ_i	chemical potential of species i
σ_i	electrical conductivity of species i
π_a	apparent/open porosity
π_t	true porosity
ρ_i	density of species i
ρ_b	bulk density
ρ_t	true density
σ_{el}	electronic conductivity
σ_{ion}	ionic conductivity
τ	shear stress

1 Introduction

Mixed ionic-electronic conducting (MIEC) ceramic membranes are growing increasingly popular within research and development [1]. As the global demand for energy is growing, and hydrocarbon reservoirs diminishing, the world is in need of a more diverse energy supply. An application area for the MIEC-membranes is therefore formed within the field of energy production. This is mainly within chemical processing, including the partial oxidation of methane to syngas [2], but also as cathodes for solid oxide fuel cells (SOFC) and anodes for solid oxide electrolysis cells (SOEC) [3].

Syngas is an intermediate product which can be further processed to a range of valued products, amongst other through the Fischer-Tropsch process to produce diesel. Traditionally, syngas is produced by the strongly endothermic steam reforming process, Eq. 1.1.

$$CH_4 + H_2O \Leftrightarrow CO + 3H_2 \tag{1.1}$$

An alternative is the slightly exothermic partial oxidation of methane, Eq. 1.2.

$$CH_4 + \frac{1}{2}O_2 \Leftrightarrow CO + 2H_2 \tag{1.2}$$

Due to requirements in a lot of downstream processes where syngas products are used, the syngas is required to be of high purity. A criteria for a high purity syngas product starts with a clean source of oxygen, and using a cryogenic oxygen supply is very energy costly [4].

An alternative route is the use of MIEC-membranes. With a regular air feed, MIEC-membranes can provide a pure and energy effective supply of oxygen. Susceptible to both ionic and electronic transport, MIECs gas separating abilities are looking promising in ways of finding an economical, clean and efficient route for separation oxygen from air [2].

The flux of oxygen through a MIEC-membrane is often used as a measure of its quality. The flux can be limited by two factors, either: (i) the rate of solid state diffusion within the membrane or (ii) the interfacial oxygen exchange at either side of the surface. Down to a characteristic size, L_C, the former will be rate limiting. Below L_C, the exchange rate across the interfaces will be rate limiting [2].

Naturally, thin film membranes are showing promising results with respect to high oxygen flux. Given the thickness of the thin film membranes, and the brittle nature of ceramics, these membranes will often lack desired mechanical properties. Asymmetric membranes, consisting of a dense thin film membrane supported by a porous substrate, are believed to provide adequate strength contribution and at the same time maintain a high flux of oxygen [2].

A criteria for these porous substrates is that they shall not limit the flux of the dense membrane of which they are supporting, and today's porous substrates have not yet shown sufficient degree of gas permeability [5].

The permeability through a porous substrate will depend strongly on the pore geometry and of the tortuosity in the structure [6]. To obtain a high degree of viscous gas flow through a substrate, the pores are required to be of a size greater than that of the mean free path of the gas molecules [7].

However, the gas permeability of the porous substrates always needs to be weighed against its strength contribution. A porous substrate is desired to achieve a high flow of gas, while at the same time retaining a strong structure. Therefore, the processing of these pores needs to be optimized in order to obtain a high flux structure.

In this work, the processing of porous $La_{0.2}Sr_{0.8}Fe_{0.8}Ta_{0.2}O_{3-\delta}$ (LSFTa) substrates is addressed. The aim of this paper is to achieve highly permeating tape casted substrates with adequate strength. Uniaxial press will be used to produce porous substrates, which will be characterized with respect to porosity and permeability. The most promising substrates will be tape casted and characterized with respect to porosity, permeability and strength. The effect of the ceramic powder particle size and the pore former morphology on the permeability and substrate structure will be investigated by

i) producing substrates from coarse sized LSFTa, with an addition of fine sized LSFTa
ii) producing substrates from coarse LSFTa and carbon black pore former
iii) producing substrates from coarse LSFTa and carbon black pore former, with an addition of fine sized LSFTa
iv) producing substrates from coarse sized LSFTa and cellulose acetate pore former

2 Theory

2.1 MIEC-membrane transportation fundamentals

Owing to MIECs ability to conduct both oxygen ions and electrons, the membranes can operate without the need of electrodes and external circuitry [1, 2]. Oxygen separation using a MIEC-membrane exploits a difference in oxygen partial pressure imposed across the membrane. In a typical membrane reactor, this can be achieved by exposing the membrane to an air feed on one side, while depleting the oxygen partial pressure by a chemical reaction on the other, i.e. the autocatalytic reaction of methane to syngas [1, 2]. The partial pressure difference experienced by the membrane under such circumstances is illustrated in Figure 2-1[2].

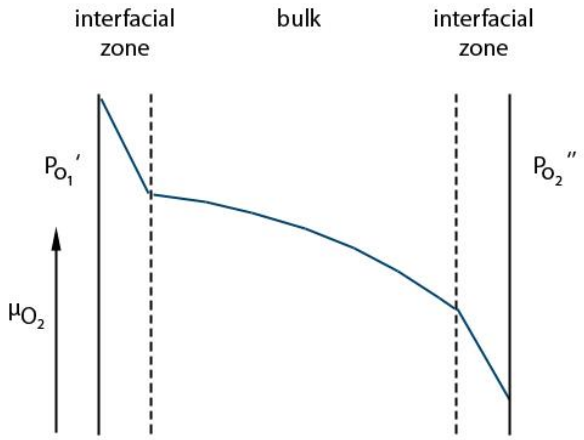

Figure 2-1: Illustration of oxygen partial pressure gradient across the MIEC-membrane while experiencing an air feed on one side, with a continuous depletion of oxygen by a chemical reaction on the other. Redrawn from [2].

Assuming a crack free and dense membrane, the permeation of oxygen molecules is rendered impossible. Instead, oxygen gas is dissociated and ionized at the oxide surface, where electrons are picked up from accessible electronic states at the surface. Ionized oxygen ions are transported across the dense membrane via oxygen vacancies in the structure, and recombined to form oxygen molecules on the low-pressure side. The flux of oxygen ions is charge compensated by the movement of electronic charge carriers, moving simultaneously in the opposite direction [2]. Charge transfer within a MIEC-membrane, producing syngas with oxygen from air feed, is schematically shown in Figure 2-2 [1].

The interaction between the oxygen molecules and the ceramic membrane can be represented by (using Kröger-Vink notation):

$$\frac{1}{2}O_2 + V_o^{\cdot\cdot} + 2\,e' \Leftrightarrow O_o^x \tag{2.1}$$

where $V_o^{\cdot\cdot}$ denotes an oxygen vacancy. Here, oxygen vacancies are the mobile ionic defects [2].

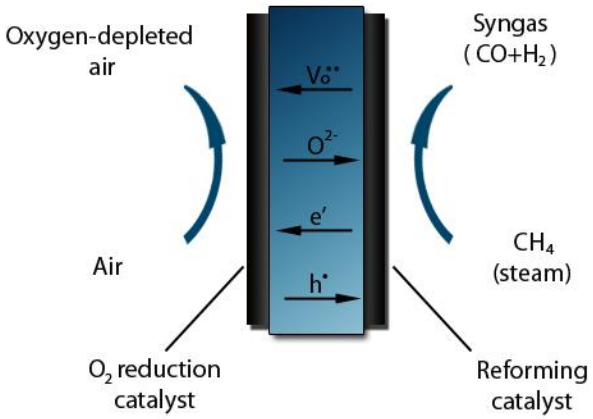

Figure 2-2: Charge and mass transport within a MIEC-membrane, producing syngas from methane, while transferring oxygen from the air feed side. Redrawn from [1].

The rate at which oxygen permeates through a dense membrane is essentially controlled by two factors: the rate of solid state diffusion within the membrane, and that of interfacial oxygen exchange on either side of the membrane [2]. If bulk diffusion is limiting, the flux can be described by the Wagner equation, Eq. 2.2 [1, 2]

$$J_{O_2} = -\frac{1}{4^2F^2h}\int_{lnP''_{O_2}}^{lnP'_{O_2}} \frac{\sigma_{el}\sigma_{ion}}{\sigma_{el}+\sigma_{ion}}\,dlnP_{O_2} \tag{2.2}$$

where σ_{ion} and σ_{el} refer to the partial ionic and electronic conductivities, F the Faraday constant and h the membrane thickness. From the Wagner equation it is clear that the oxygen flux increases with decreasing membrane thickness. For substrates of a large membrane thickness, the flux of oxygen will be limited by bulk diffusion. This will be the case until the

thickness is decreased below a characteristic value, L_C, at which the transfer across the interfaces becomes rate determining. The characteristic value, L_C, is defined as [2]

$$L_c = \frac{D_o}{k_o} \tag{2.3}$$

where D_o is the bulk self diffusion coefficient and k_o is the surface exchange coefficient [1, 2].

2.2 The perovskite structure

The ideal perovskite is an ABO_3 system, with an array of BO_6-octahedra and an interstitial A. By incorporating other elements into the structure, the characteristics of the perovskite can be tailored for its specific needs. For oxygen conducting membranes, desired characteristics are: high oxygen flux, chemical stability in both oxidizing and reducing environments and low chemical and thermal expansion [1, 2].

Several perovskite systems are being investigated with the purpose of finding suitable candidates for oxygen separation [1, 2, 8-14]. Doped $LaSrFeO_3$ (LSF) is amongst those perovskite systems which have shown promising results in terms of high oxygen flux and conductivity [15, 16].

The starting compound of LSF is $LaFeO_3$, and the dissolution of $SrFeO_3$ in to $LaFeO_3$ can be described by[2]

$$SrFeO_3 \xrightarrow{LaFeO_3} Sr'_{La} + \dot{Fe}_{Fe} + 3O_O^x \tag{2.4}$$

Charge neutrality is thereby compensated by the formation of Fe^{4+}-ions. Oxygen non-stoichiometry is then controlled by

$$2\dot{Fe_{Fe}} + O_O^x \leftrightarrow 2Fe_{Fe}^x + V_o^{\cdot\cdot} + \frac{1}{2}O_2 \tag{2.5}$$

and

$$2Fe_{Fe}^x \leftrightarrow Fe'_{Fe} + \dot{Fe}_{Fe} \tag{2.6}$$

Doping the A- or B-site with a lower valent cation leads to oxygen vacancies in the perovskite structure, which allows for the oxygen movement through the lattice [2, 10]. Already during pioneering studies it was found that an increased degree of A-cation substitution led to an increase in oxygen flux, but at the same time led to a decrease thermodynamic stability, indicating a trade-off between oxygen flux and the stability of the structure [2].

Doping the B-site in LSF with high valent Ta has shown to raise both the chemical and mechanical stability of LSF-membranes to a desired level [17, 18]. The specific composition of $La_{0.2}Sr_{0.8}Fe_{0.8}Ta_{0.2}O_{3-\delta}$ (LSFTa) is a candidate which has recently shown promising results with respect to both high oxygen flux and structural stability [4, 5, 17].

2.3 Gas flow in porous substrates

Due to the fact that the flux of oxygen through a MIEC-membrane increases with decreasing thickness down to its critical thickness, there has been a growing interest for asymmetric membranes [2]. Asymmetric membranes consist of a dense membrane deposited on a porous support substrate. Deposition of thin films on porous substrates is expected to combine the high mechanical strength from the porous substrate, while maintaining the high oxygen flux and chemical abilities of the dense membrane [2]. It is then of course crucial that the gas flow through the porous support does not limit the flux of oxygen through the dense membrane [19]. Compatibility problems between the two layers can be avoided by producing a support of the same composition as the dense membrane [2].

Producing porous supports can be achieved by the use of pore formers. Pore formers are mixed into the green body and burned off, leaving the substrate with small, homogeneously dispersed and connected pores throughout the structure. Carbon black and cellulose acetate are pore formers which have shown promising results with respect to such connected porosity for similar membranes [11, 20-22].

Permeability is a measure of flow through the porous substrate. Gas flow through a porous medium can be a complex combination of viscous flow, Knudsen diffusion, and binary-diffusion. Each gas molecule might be transported by any of these three mechanisms, but which of these three which will be the dominating transport mechanism will depend on pore size and absolute pressure in the pore [23].

The Knudsen-regime is a result of the pore size being smaller than the mean free path of gas molecules transported, where transport is controlled by molecule-wall interactions. Binary

diffusion and viscous flow occurs when the pore size is much larger than the mean free path of the molecules. In the case of viscous flow, molecule-molecule interactions will dominate the flow. Diffusive transport will be controlled by a concentration gradient, while viscous flow is bulk flow caused by pressure gradients [23].

A porous substrate's gas permeability will depend strongly on the degree of tortuosity, where the tortuosity is defined as a ratio of the actual path length of a pore to the thickness of the porous medium [23]. The amount of gas passing through the porous substrate is proportional to the permeability, the substrate's surface area and the pressure difference, while being inversely proportional to the substrate thickness and to the gas viscosity by [24]

$$\frac{V}{t} = \frac{D \cdot A \cdot \Delta p}{h \cdot \eta} \tag{2.07}$$

where

V = volume of the gas (m^3)
t = period of time (s)
D = gas permeability (Perm) = ($10^{-4} m^2$)
A = surface area of the substrate (m^2)
h = substrate thickness (m)
Δp = pressure difference across substrate (N/m^2)
η = gas viscosity (10^{-1}kg/m s)

The air permeability, D_a, can be calculated if the air flow rate through a given capillary is known. Gas permeability can be measured using the RDC-145 air permeability apparatus, where gas permeability is determined by measuring the time a gas needs to pass through the porous substrate, in order to refill a partly evacuated system. The RDC-145 Air permeability measurement system is based on a factor K which defines air flow according to Eq. 2.08 [24]

$$K = \frac{V}{t \cdot \Delta p} \tag{2.08}$$

The permeability can then be determined by inserting Eq. 2.08 into Eq. 2.07, resulting in [24]

$$D_a = \eta_a \cdot \frac{h}{A} \cdot K \tag{2.09}$$

The RDC-145 Air permeability apparatus is intended for samples of a specific geometry (height=0.02m, Ø=0.05m). For samples of a different geometry, it is possible to use a modified sample holder and recalculate the air permeability based on the new sample geometry.

A picture of the modified sample holder can be seen in Figure 2-3a) and a schematic of its inside structure can be seen in Figure 2-3b). The schematic shows how the substrate is placed in the middle of the cylinder with four different sealing layers on each side of the substrate. When all layers are put in the correct order, the layers are screwed together by the handle seen on the top of the cylinder in Figure 2-3a).

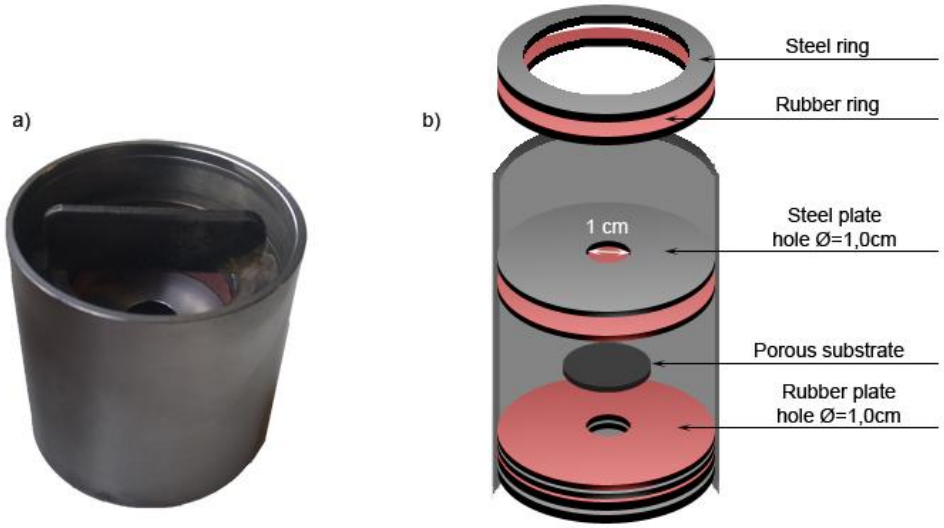

Figure 2-3: a) Picture showing the modified sample holder with the locking mechanism on the top of the steel cylinder. b) A schematic of the modified sample holder and its different sealing layers. The substrate is in the middle and air flow is limited to a circular area of Ø=1,0cm on the substrate

Air permeability measurements using this modified sample holder can be calculated according to

$$D_{a\,(real)} = D_{a(1)} \cdot \frac{A_1}{h_1} \cdot \frac{h_2}{A_2} \tag{2.10}$$

where $Da_{(1)}$ is the permeability calculated by the RDC-145, A_1 is the area $\pi(0.025\text{m})^2$, h_1 is the thickness 0.02m, A_2 is the exposed area of the substrate and h_2 is the substrate thickness.

After measuring the permeability of the porous substrate, the flux of oxygen can be calculated according to Eq. 2.07, by assuming a low pressure difference, Δp, across the substrate.

The flux at operating temperature (800 – 1000 °C) can then be estimated by adjusting the flux according to the change in gas viscosity as the temperature increases. Viscosities of air at elevated temperatures used in these estimations are calculated by Kadoya et. al. [25].

2.4 Measuring porosity of porous substrates

The bulk density, apparent porosity and true porosity of a porous substrate can be measured using the Archimedes method following the international standard ISO 5017:1998(E). These parameters are calculated by measuring the substrate's dry weight, weight immersed in liquid and weight in air with immersed liquid still remaining inside the porous substrate.

The bulk density, ρ_b, is a ratio of mass to bulk volume of a material while dry, expressed in grams per cubic centimeter or in kilograms per cubic metre

$$\rho_b = \frac{m_1}{m_3 - m_2} \cdot \rho_{liq} \tag{2.11}$$

where m_1 is the dry weight of the substrate, m_2 is the weight of the substrate immersed in liquid and m_3 the weight of substrate in air with immersed liquid still inside the porous substrate. The apparent porosity, π_a, is the ratio of total volume of open pores to the bulk volume of the sample body, expressed as a percentage of bulk volume

$$\pi_a = \frac{m_3 - m_1}{m_3 - m_2} \cdot 100 \tag{2.12}$$

The true porosity, π_t, is the ratio of the total volume of pores, including both open and closed pores, to the bulk volume of the sample body, also expressed as a percentage of bulk volume

$$\pi_t = \frac{\rho_t - \rho_b}{\rho_t} \cdot 100 \tag{2.13}$$

where ρ_t is the true density of the material, expressed in grams per cubic centimeter or in kilograms per cubic metre.

2.5 Producing ceramics by tape casting

Tape casting is a ceramic processing method used to create thin films of ceramic tape. A slip of ceramic powder is poured onto a Mylar film. As the film is pulled in the roller direction, the slip is limited by a doctor blade, where the height of the blade sets the thickness of the tape. The process is illustrated in Figure 2-4.

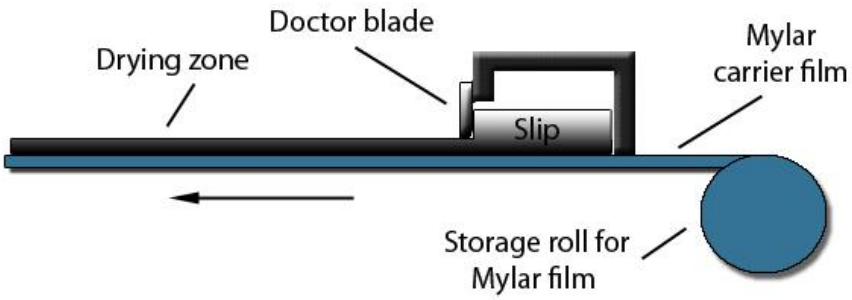

Figure 2-4: Illustration of ceramic tape produced by tape casting

A high concentration of ceramic powder in a stable slip is required for a successful product. The high concentration is desired to avoid excessive shrinkage. Also, the slip's viscosity needs to be high enough to establish a stable tape on the carrier sheet, and at the same time be of low enough viscosity to flow [26].

A quality tape cast needs to fulfill several criteria in order to make a good final product, such as [27]

i) No defects during drying
ii) Cohesion to allow manipulation of dried sheets
iii) Microstructural homogeneity
iv) Easy pyrolysis (burnout)
v) High mechanical strength after sintering

Various additives are therefore needed to obtain the desired characteristics of the tape casting slurry and of the tape after drying. However, all additives have to be removed from the green body prior to sintering. For ceramic processing using a large additive content, such as tape casting, the removal of additives is often a crucial step in the fabrication process [26].

The mixing of the tape casting slurry is often done in two steps. First, ceramic powder is mixed with water and a dispersant. The dispersant is added to separate ceramic particles and thereby avoiding agglomeration of particles [27].

Darvan-C is an organic dispersion agent used in ceramic processing to obtain stable slips by electrosteric stabilization of ceramic particles. Electrosteric stabilization is used to counter the attractive van der Wall forces between ceramic particles in colloidal ceramic processing, and requires the presence of adsorbed polymers and a significant double layer repulsion [26].

2. THEORY

To achieve a stable suspension, a critical amount of polymer is required. This critical amount corresponds to the amount of polymer needed to obtain full coverage of the particles. At this point, the stability of the suspension is maximized and the viscosity of the suspension goes through a minimum. Adding more polymer above this point will only serve to produce excess burn off material, and is revealed by an increase in viscosity [26].

From similar research [28-30] an approximate amount of Darvan-C, with respect to the powder surface area, 0.31mg/m^2 is suggested as optimum amount for stabilization. The optimum amount for stabilization of spray pyrolysed LSFTa has previously been determined to be 1.85 wt% of the powder [13].

The flow behavior of the slip can be measured by rheological measurements. The viscosity, η, of a liquid is defined as

$$\eta = \frac{\tau}{\dot{\gamma}} \tag{2.18}$$

where τ is the shear stress and $\dot{\gamma}$ the shear rate. However, most colloidal suspensions will be non-Newtonian (dependent of shear rate) and the viscosity $\eta(\dot{\gamma})$ must be defined

$$\eta(\dot{\gamma}) = \frac{d\tau}{d\dot{\gamma}} \tag{2.19}$$

where the viscosity at a given strain rate is found from the slope of the curve of shear stress versus strain rate [26].

After the ceramic particles have been stabilized in the slurry, more additives are added and the slurry is mixed to achieve homogenization. Binder is added to the slurry to provide the green body with strength, making it possible to handle when dried, while plasticizers are added to soften the binder, making the tape more flexible and easier to manipulate [27].

2.6 Strength of porous substrate

Mechanical strength of ceramic substrates can be measured by using the Instron 5543. This test method is called the ball-on-ring test, where a force is exerted by a ball on a disc sample until fracture. The fracture load is recorded and a biaxial strength can be calculated from the substrate geometry, according to Eq. 2.20 [31].

$$S_{max} = \frac{3 \cdot F_N \cdot (1+v)}{4 \cdot \pi \cdot t^2}\left[1 + 2\ln\left(\frac{a}{b}\right) + \left(\frac{1-v}{1+v}\right)\left(\frac{a}{R}\right)^2\left(1 - \left(\frac{b^2}{2a^2}\right)\right)\right] \quad (2.20)$$

where S_{max} = Biaxial strength (MPa)

F_N = Fracture load (N)

v = Poisson's ratio (-)

t = Substrate thickness (µm)

a = Radius of the support (mm)

b = Effective contact radius between sample and ball (mm)

R = Sample radius including overhang (mm)

The biaxial strength measurement allows for testing of substrates which are similar to the desired final product. Also, it makes a more relevant loading configuration to actual service configuration compared to what uniaxial loading does [31]. A biaxial strength of 34MPa has been reported for similar porous substrates intended for MIEC-membrane supports [32].

3 Experimental

3.1 Chemicals and apparatus

3.1.1 Chemicals

Coarse LSFTa-powder was synthesized by solid state reaction. Chemicals used during this synthesis, their formula, supplier and purity can be seen in Table 3-1.

Table 3-1: List of chemicals used during solid state synthesis, their formula, supplier and purity

Chemical	Formula	Supplier	Purity (%)
Strontium carbonate	$SrCO_3$	Alfa Aesar GmbH & Co.KG	99.4
Lanthanum(III) oxide	La_2O_3	Merck KGaA	99
Tantalum(V) oxide	Ta_2O_5	Alfa Aesar GmbH & Co.KG	99
Iron(III) oxide	Fe_2O_3	VWR International AS	99
Ethanol	CH_3CH_2OH	VWR International AS	99.8

Fine LSFTa-powder produced by spray pyrolysis was supplied by PhD-student Ørjan Fossmark Lohne. Synthesis route and chemicals used during spray pyrolysis synthesis can be seen in appendix B1 and B2.

During the forming of green bodies, several additives were used to obtain desired characteristics. Additives used during the forming of these green bodies, their purpose and supplier can be seen in Table 3-2. Densities of the pore formers are 1.8 – 2.1g/cm^3 and 1.3g/cm^3 for carbon black and cellulose acetate respectively, reported by suppliers.

Table 3-2: List of additives used in the forming of green bodies, their purpose and supplier

Additive	Supplier	Purpose
Darvan-C (25%)	R.T. Vanderbilt Company, Inc.	Dispersant
Charcoal activated	Merck KGaA	Pore former
Cellulose acetate	Sigma-Aldrich Norway AS	Pore former
BYK 3455	Altana, BYK additives & instruments	Plasticizer
BYK 3955 P	Altana, BYK additives & instruments	Carbon black dispersant
Duramax B 1000	Duramax	Binder
Duramax B 1235	Duramax	Binder

3.1.2 Apparatus

Table 3-3 shows the different apparatus, specified by model and application area, used during this work.

Table 3-3: List of apparatus, their specification and application, used during this work

Apparatus	Specification	Application
Furnaces	Entech HT2 Chamber furnace	Sintering
	Entech SF4 Chamber furnace	Calcination
SEM	LV-SEM Hitachi S-3400N	Surface characterization
		Powder morphology analysis
BET	Micromeritics Tristar 3000	Surface area analysis
XRD	AXS D8Focus	Study of phase composition
TGA	Netzsch STA 449C	Thermal analysis
DIL	Netzsch DIL 402C	Sintering analysis
Malvern	Mastersizer 2000	Particle size distribution analysis
Viscosimeter	HAAKE Mars III (CCTi27)	Study of rheological properties
Ball-on-ring	Instron 5543	Fracture strength measurement
Air permeability	RDC-145	Permeation measurement
Planetary mill	Retsch PM 100	Crushing and mixing of powder

3.2 Procedure

3.2.1 Synthesis and characterization of $La_{0.2}Sr_{0.8}Fe_{0.8}Ta_{0.2}O_{3-\delta}$

The oxides La_2O_3, Fe_2O_3 and Ta_2O_5 were calcined (800 °C, 24h) in three different crucibles (Al_2O_3) with a heating and cooling rate of 200 °C/h. Heat program can be seen in Figure 3-2. $SrCO_3$ was standardized (5 °C/min, max 1000 °C) using Netzsch STA 449C (TGA).
The calcined oxides and the raw $SrCO_3$ were used in the solid state synthesis of coarse LSFTa. A flowchart showing the synthesis process is shown in Figure 3-1.

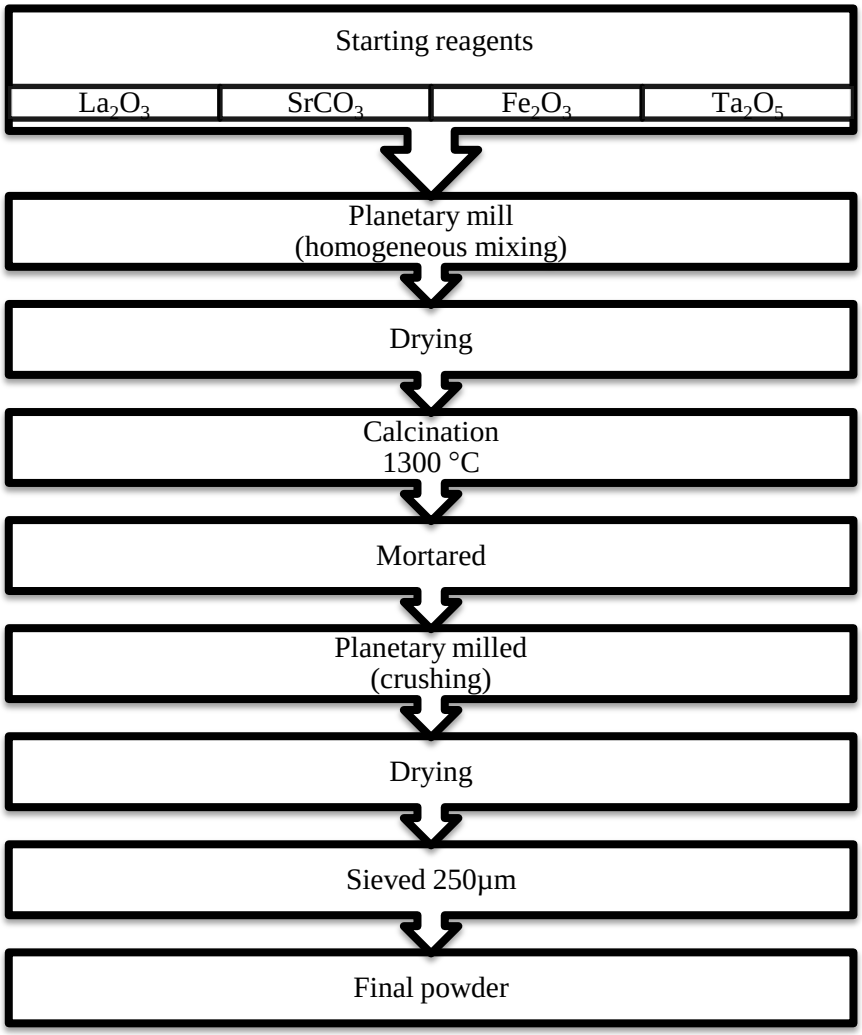

Figure 3-1: Flowchart showing the synthesis of coarse LSFTa by solid state reaction

Calcined oxides and as received $SrCO_3$ were weighed and mixed by $La_{0.2}Sr_{0.8}Fe_{0.8}Ta_{0.2}O_{3-\delta}$-stoichiometry. The exact amount of the different components is shown in Table 3-4. Mixed powder, EtOH (100%) and ZrO_2-grinding balls (70 balls, Ø10mm) were added to a ZrO_2-container (250ml) and mixed by planetary mill (150 rpm, 1h).

Table 3-4: Amounts of the different components in powder mixed for solid state synthesis of $La_{0.2}Sr_{0.8}Fe_{0.8}Ta_{0.2}O_{3-\delta}$

Component	La_2O_3	$SrCO_3$	Fe_2O_3	Ta_2O_5
Amount (g)	14.37	50.94	28.17	19.48

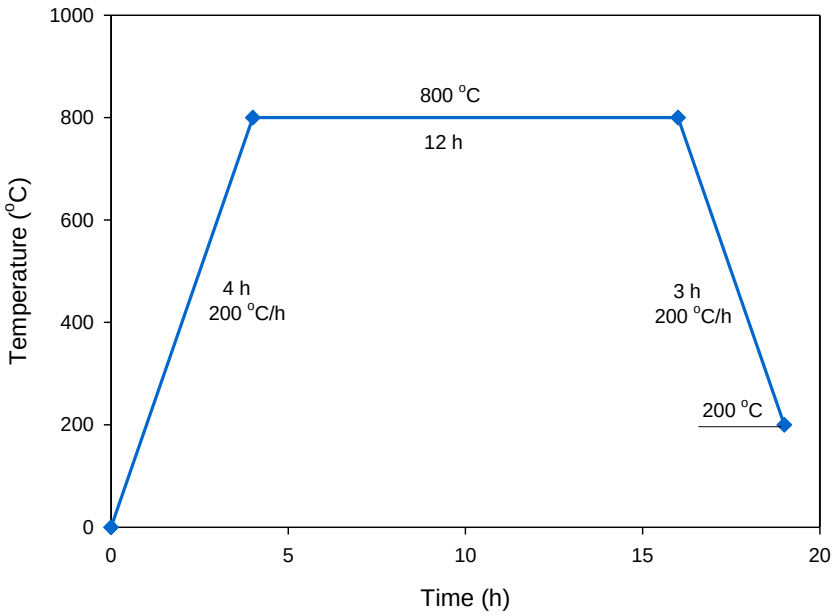

Figure 3-2: Heat program used for calcination of La_2O_3, Fe_2O_3 and Ta_2O_5

The homogenous solution was dried in a rotavapor, placed in an alumina crucible with an alumina lid, and calcined (1300 °C, 12h), with a heating and cooling rate of 200 °C.

LSFTa-powder was subsequently mortared and sieved (250µm), added with EtOH (150ml, 100%) and ZrO_2-grinding balls (70 balls, Ø10mm) to a ZrO_2-container (250ml) and crushed (planetary mill, 150 rpm, 2h) until desired coarse particle size (d≈20) was achieved.

A sample (3ml) of homogenous solution was pipetted from planetary mill container and into a sample glass (10ml) for particle size distribution analysis. Milled LSFTa was dried in a rotavapor and collected.

Sample from planetary mill was sonicated (10% intensity, 30s) by ultrasound finger to avoid any agglomerates. Particle size distribution of sonicated sample was analyzed by laser diffraction technique in aqueous media, using Malvern Mastersizer 2000.

Phase purity was controlled by an X-ray diffraction spectrum of the LSFTa-powder, achieved by scanning in the 2θ region from 20° and 60°, with a step size of 0.01° and step time of 0.5s, using AXS D8 Focus.

Surface area analysis of solid state and spray pyrolysed powder was performed by drying small samples (1.5g) of each powder overnight (250 °C, 40mbar, 24h) and analyzed by BET-analysis, using Tristar 3000.

Morphology of solid state and spray pyrolyzed powder was characterized by using Hitachi S-3400N scanning electron microscope (SEM). Small amounts of solid state and spray pyrolysed powder (<0.5g) were dispersed in EtOH (100%, 3ml). A droplet from each glass was left to dry on two SEM-platforms and imaged by SEM.

DIL-analysis of solid state powder and spray pyrolysed powder was carried out (5 °C/min, max 1000 °C), using Netszch DIL 402C, to reveal the sintering characteristics of the two powders.

3.2.2 Characterization of pore formers

Carbon black and cellulose acetate are the pore formers investigated in this work. The pore formers morphology was characterized by SEM. Small amounts of cellulose acetate and carbon black (<0.01g) were dispersed in two different sample glasses (10ml) with iso-propanol (3ml). A droplet from each sample glass was left to dry on two SEM-platforms and imaged by SEM.

Ash contents of the two pore formers was analyzed by burning off two small samples (≈1g) of each pore former. Four crucibles (Al_2O_3, Ø15mm) were heated to 800 °C and further cooled to 100 °C in a furnace, at which point the crucibles were removed from the furnace and weighed. Two crucibles were added a sample (1g) of carbon black and the other two crucibles were added a sample (1g) of cellulose acetate. The samples were heated (800 °C) and further cooled to 100 °C in a furnace, at which point the crucibles were removed from the furnace and weighed once again. Ash content was calculated from increase in mass.

3.2.3 Investigating optimum amount of dispersant

Three different solutions with varying dispersant contents were made in order to analyze the optimum amount of dispersant. The selected range of dispersant (0.2 - 0.6 wt%) was chosen from the estimated amount of 0.31mg/m^2, suggested by literature [28-30].

Coarse LSFTa, dispersant (1/10 Darvan-C), distilled water and ZrO_2-balls (40 balls, Ø10mm) were added to three different bottles (PE, 100ml). Specific contents of the three different solutions are shown in Table 3-5.

Table 3-5: Contents of three different solutions for investigating optimum dispersant content

Samples, by Darvan-C content	0.2 wt%	0.3 wt%	0.4 wt%	0.6 wt%
Coarse LSFTa (g)	10.000	10.000	10.000	10.000
Water (g)	6.169	6.079	5.989	5.809
Darvan-C (g)	0.200	0.300	0.400	0.600

All samples were sonicated (10% intensity, 60s) and viscosities of the four solutions were measured by HAAKE Mars III viscosimeter (CCTi27 geometry). Viscosity values were recorded by using controlled shear stress (CS) mode at low shear range, and controlled shear rate (CR) above $30s^{-1}$ and up to $500s^{-1}$, with a dwell time of 30s at maximum shear.

3.2.4 Producing porous substrates by uniaxial pressing

Uniaxial pressing was used to screen samples of different substrate compositions in this thesis. These pellets were used for permeability measurements and to give a quick indication of the substrates' porosity and permeability.

Three porous substrates were made coarse LSFTa without the use of pore formers. These substrates were added a varying degree of fine LSFTa (SA), to investigate any effect on the sintering behavior. The three substrate compositions and their abbreviations are

1. Coarse LSFTa with 5% coverage of fine LSFTa (LSFTa_05SA)
2. Coarse LSFTa with 10% coverage of fine LSFTa (LSFTa_10SA)
3. Coarse LSFTa with 20% coverage of fine LSFTa (LSFTa_20SA)

Three porous substrates were made from coarse LSFTa and with carbon black and cellulose acetate as pore formers. These three substrates and their abbreviations are

1. Coarse LSFTa and carbon black (CB) pore former (LSFTa_32CB)
2. Coarse LSFTa and carbon black pore former, with fine LSFTa (LSFTa_32CB_20SA)
3. Coarse LSFTa and cellulose acetate (CA) pore former (LSFTa_32CA)

The amounts of pore former and fine LSFTa added, relative to that of coarse LSFTa, are listed in Table 3-6.

Table 3-6: Composition of three porous substrates made from coarse LSFTa and pore formers

Sample abbreviation	LSFTa_32CB	LSFTa_32CB_20SA	LSFTa_32CA
Pore former added	32 vol% CB	32 vol% CB	32 vol% CA
Fine LSFTa coverage (%)	-	20	-

A flowchart showing the forming process of pressed substrates can be seen in Figure 3-3. The fabrication procedure of each of these substrates is described in the following chapter.

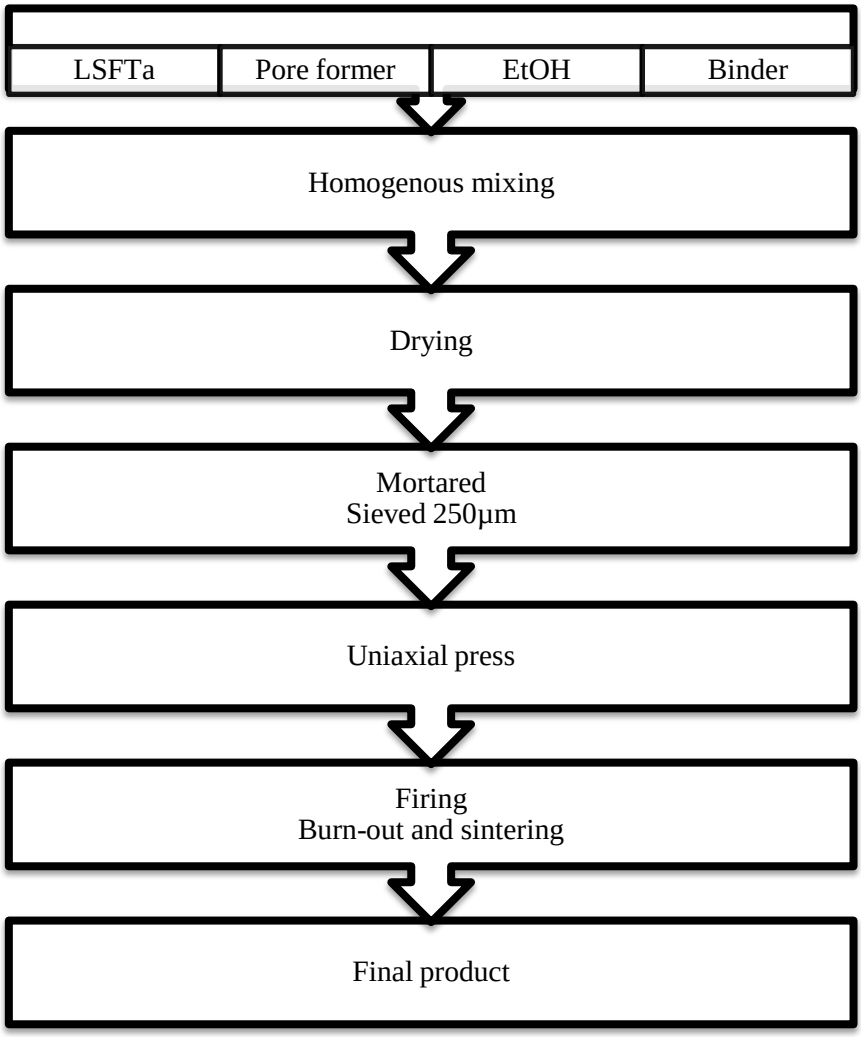

Figure 3-3: Flowchart showing the forming process of porous substrates made by uniaxial press

Porous substrates from coarse LSFTa and fine LSFTa added as sintering aid

Three samples with varying amounts of fine powder relative to that of coarse powder were produced.

A total surface area of one specific amount of coarse powder was calculated from BET-surface analysis, and a specific mass of fine particles needed to achieve a varying degree of coverage of that surface area (5%, 10% and 20% coverage respectively) was calculated. Surface areas (Sa) from BET-analysis of the two different powders are shown in Table 3-7.

Table 3-7: Surface areas from BET-analysis of coarse and fine $La_{0.2}Sr_{0.8}Fe_{0.8}Ta_{0.2}O_{3-\delta}$

	Coarse particles	Fine particles
Sa (m^2/g)	0.5368	11.3494

Spray pyrolysed particles were added to enhance the sintering abilities and thereby the strength of the substrate. Calculation of spray pyrolysed powder needed to achieve varying coverage of coarse particles can be found in appendix C1.

Solid state LSFTa, varying amounts of spray pyrolysed LSFTa, distilled water (10ml), ZrO_2-balls (12 balls, Ø5mm) and dispersant (1/10 Darvan-C) were added in three different PE-bottles (50ml). The specific compositions of the three different samples are shown in Table 3-8.

Table 3-8: Compositions of three different samples used to analyze the effect of fine $La_{0.2}Sr_{0.8}Fe_{0.8}Ta_{0.2}O_{3-\delta}$ as sintering aid

Sample	Solid state LSFTa (g)	Coverage (%)	Spray pyrolysed LSFTa (g)	Darvan-C (g)
LSFTa_05SA	5.000	5	0.012	0.0102
LSFTa_10SA	5.000	10	0.024	0.0104
LSFTa_20SA	5.000	20	0.048	0.0109

The three different solutions were mixed by ball mill (60rpm, 30min) and dried by a rotavapor. Dried powder was collected and one pellet (0.5g powder, Ø5mm) of each powder was pressed by uniaxial press (40MPa, 2min).

A sintering temperature of 1200 °C was chosen from DIL-analysis, in order to control the sintering process to only affect the fine particles. A slow heating rate up to 340 °C was chosen

to avoid any stress from burned off dispersant. The complete sintering program is presented in Figure 3-4.

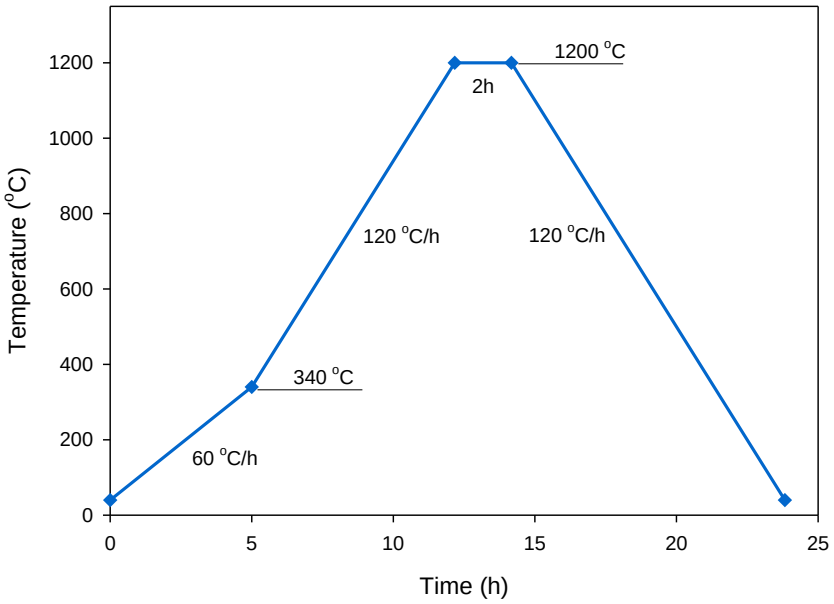

Figure 3-4: Heat program used for sintering pellets made from a combination of coarse $La_{0.2}Sr_{0.8}Fe_{0.8}Ta_{0.2}O_{3-\delta}$ and fine $La_{0.2}Sr_{0.8}Fe_{0.8}Ta_{0.2}O_{3-\delta}$

Porosity of sintered pellets was measured by Archimedes method and their structures were characterized by use of SEM.

Porous substrates from coarse LSFTa and carbon black pore former

Coarse LSFTa, pore former (carbon black), binder (1/20 ethyl cellulose) and EtOH (100%) was mixed in a sample glass (20ml). Table 3-9 shows the exact amount of the different components. The specific carbon black and ethyl cellulose content was set from previous work carried out with similar samples[13, 33].

Table 3-9: Composition of LSFTa_32CB pressed substrate

LSFTa_32CB	
Solid state LSFTa (g)	5.000
Carbon black (g)	0.500
Ethyl cellulose (g)	3.000
EtOH (g)	4.5

The content was roughly shaken (5min) and the solution was dried on an agate mortar. Dried powder was mortared and sieved (250µm). Sieved powder (2x2.5g) was pressed (40MPa, 2min) into two disc shaped pellets (Ø25mm). One pellet was sintered at 1275 °C according to Figure 3-5, while the second pellet was sintered at 1350 °C according to Figure 3-6.

Porous substrates from coarse LSFTa and carbon black pore former, with fine LSFTa added as sintering aid

Coarse LSFTa, fine LSFTa, pore former (carbon black), binder (1/20 ethyl cellulose) and EtOH (100%) was mixed in a sample glass (20ml). The carbon black and ethyl cellulose content was selected to correspond to the previously made substrates, adjusted with respect to the added fine particles. Table 3-10 shows the exact amount of the different components.

Table 3-10: Composition of LSFTa_32CB_20SA pressed substrate

LSFTa_32CB_20SA	
Solid state LSFTa (g)	5.000
Spray pyrolysed LSFTa (g)	0.1440
Carbon black (g)	0.5048
Ethyl cellulose (g)	3.0288
EtOH (g)	4.5

The content was roughly shaken (5min) and the solution was dried on an agate mortar. Dried powder was mortared and sieved (250µm). Sieved powder (2x2.5g) was pressed (40MPa, 2min) into two disc shaped pellets (Ø25mm). One pellet was sintered at 1275 °C according to Figure 3-5, while the second pellet was sintered at 1350 °C according to Figure 3-6.

Porous substrates from coarse LSFTa and cellulose acetate pore former

Coarse LSFTa, pore former (cellulose acetate), binder (1/20 ethyl cellulose) and EtOH (100%) was mixed in a sample glass (20ml). The amount of cellulose acetate added was calculated from density to obtain the same volume equal to that of carbon black used in previous samples. Table 3-11 shows the exact amount of the different components.

Table 3-11: Composition of LSFTa_32CA pressed substrate

LSFTa_32CA	
Solid state LSFTa (g)	5.000
Cellulose acetate (g)	0.333
Ethyl cellulose (g)	3.000
EtOH (g)	4.5

The content was roughly shaken (5min) and the solution was dried on an agate mortar. Dried powder was mortared and sieved (250µm). Sieved powder (2x2.5g) was pressed (40MPa, 2min) into two disc shaped pellets (Ø25mm). One pellet was sintered at 1275 °C according to Figure 3-5, while the second pellet was sintered at 1350 °C according to Figure 3-6.

3.2.5 Sintering of pressed porous substrates

TGA of LSFTa mixed with cellulose acetate and LSFTa mixed with carbon black was performed (5 °C/min, max 1000 °C). A slow heating rate up to 440 °C and intermediate dwell temperatures were added to the sintering program as a result of TGA. Intermediate dwell temperatures were added at 270 °C for samples containing cellulose acetate and 440 °C for samples containing carbon black. A sintering temperature of 1275 °C was selected from previous work [33].

An increased sintering temperature of 1350 °C was chosen after analyzing substrates sintered at 1275 °C. Structures of the sintered samples were characterized by SEM.

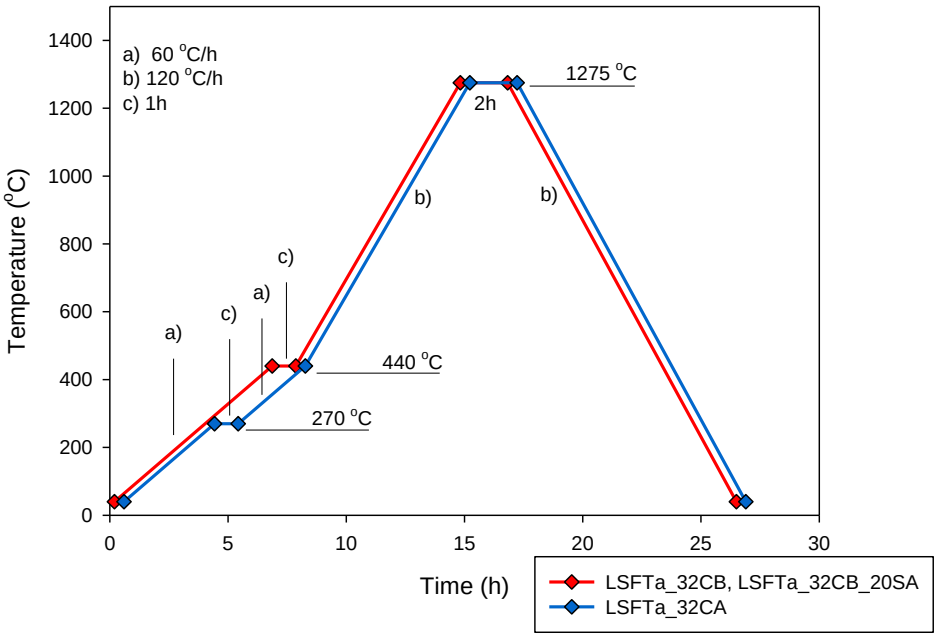

Figure 3-5: Sintering program for porous substrates made by uniaxial press sintered at 1275 °C. The red line represents the sintering program used for substrates made with carbon black pore former, while the blue line represents the sintering program used for substrates made with cellulose acetate

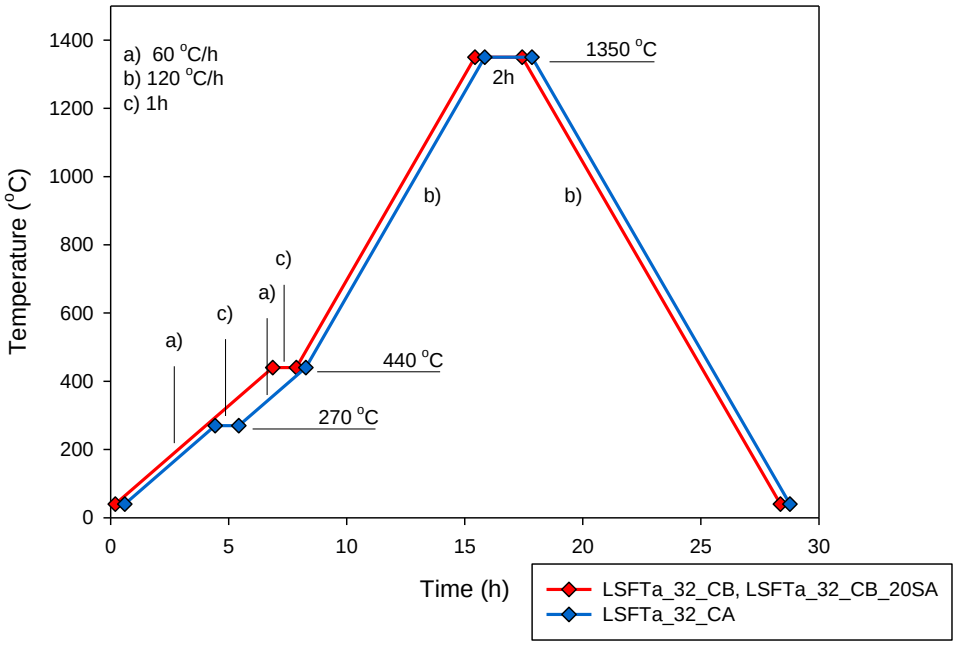

Figure 3-6: Adjusted sintering program with maximum temperature of 1350 °C. The red line represents the sintering program used for substrates made with carbon black pore former, while the blue line represents the sintering program used for substrates made with cellulose acetate pore former

3.2.6 Porosity measurements of pressed porous substrates

Apparent porosity of the three different substrates sintered at 1275 °C and 1350 °C was measured by the Archimedes method according to the ISO-standard 5017:1998(E). Substrates were dried in a low temperature furnace (110 °C, 2h) and dry weight (m_1) was measured. Dried substrates were moved to a pressure chamber and pressure was reduced (20mbar, 15min). Substrates were immersed in liquid (iso-propanol) while kept under reduced pressure (25mbar, 30min). The immersed substrates were removed from the evacuated chamber and weighed while immersed (m_2) and in air while wet (m_3). Apparent porosity of substrates was then calculated.

3.2.7 Permeability measurements of pressed porous substrates

Permeability of the three different pore former substrates sintered at 1275 °C and 1350 °C was measured by the use of a RDC-145 Air permeability apparatus. The porous substrates were mounted in a modified sample holder and the permeability was measured by measuring the time a gas needs to pass through the substrates in order to fill a partly evacuated system.

3.2.8 Producing porous substrates by tape casting

The fabrication and characterization of porous substrates without pore former was not further pursued due to poor gas permeating structures. The three previous porous substrates made with added pore former in 3.2.4, seemed promising with respect to both porosity and permeability. Therefore, the same compositions were also produced by tape casting. A flowchart showing the tape casting process can be seen in Figure 3-7. The fabrication of each of these tape casts is described in the following chapter.

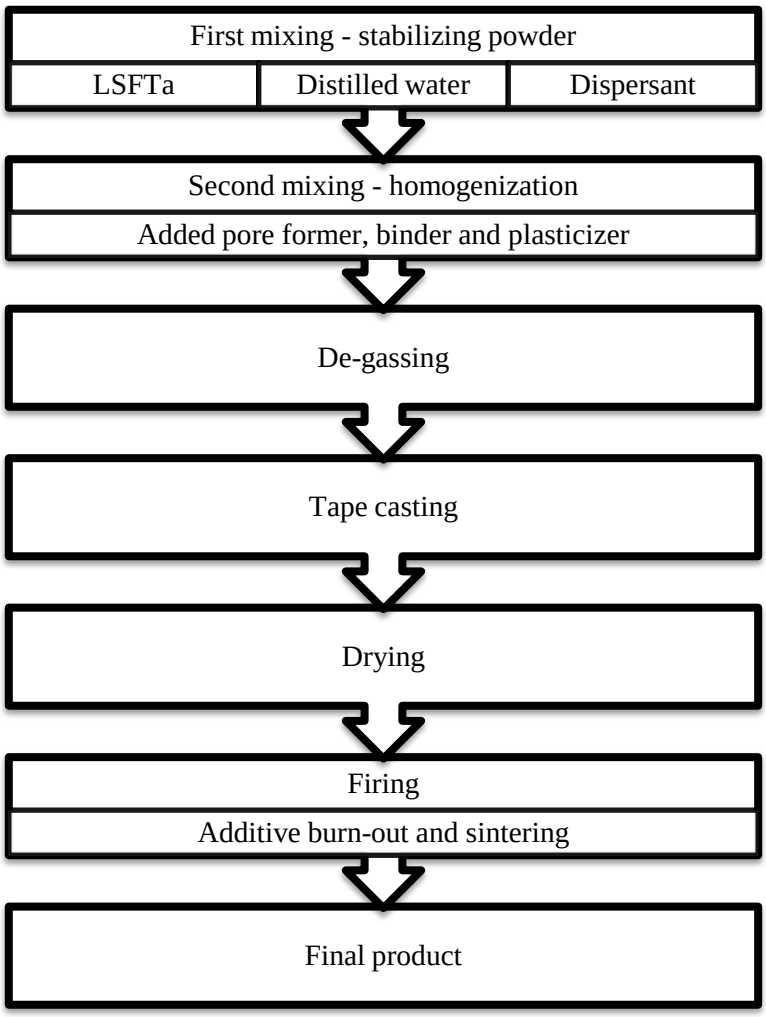

Figure 3-7: Flowchart of tape casting process

The tape casting of porous substrates was made with various amounts of additives. The binder and plasticizer contents were suggested by co-supervisor Dr. Jonas Gurauskis. The binder contents were adjusted after the first tape cast and the remaining tape casts were all based on this specific composition.

The first tape cast held a smaller quantity of LSFTa as it was intended as a test slurry, and some adjustments in the additive contents was expected. The height of the doctor blade was also adjusted after performing the first test, in order to obtain a certain thickness of the final products. After the first tape cast, the height was set to 1000µm for all remaining composition.

Tape casting of coarse $La_{0.2}Sr_{0.8}Fe_{0.8}Ta_{0.2}O_{3-\delta}$ and carbon black pore former

Coarse LSFTa, dispersant (1/10 Darvan-C), distilled water and ZrO_2-balls (3 balls, Ø10mm) were added to a bottle (PE, 125ml). Optimum amount of dispersant was selected from previously performed rheological measurements.

The ceramic particles were stabilized in water by slow rolling (≈30rpm, 4h)

Pore former and processing additives were added to the bottle and homogenization was achieved by slow rolling (≈30rpm, 24h). Slurry contents and specified processing additives used can be seen in Table 3-12.

Table 3-12: Contents of first tape casting slurry w/ 32 vol% carbon black as pore former

LSFTa_32CB			
Coarse LSFTa		10.000g	
Carbon black		1.000g	
Distilled water		2.200g	
Processing additives used			
Darvan-C	0.2 wt% of LSFTa	0.200g	Dispersant
Duramax B1000	7.5 wt% of total powder	0.825g	Binder
Duramax B1235	7.5 wt% of total powder	0.825g	Binder
BYK 3455	7.5 wt% of total slurry contents	1.129g	Plasticizer

Due to poor rheological behavior the binder contents of B1000 and B1235 was increased (15 wt% and 10 wt% of total powder respectively). Solution was slow rolled further (24h) to achieve homogenization, and final tape casting slurry was tape casted (height180 µm, R.T., 60% speed).

The original composition was adjusted for a new tape cast based on the previous attempt.

Due to an inhomogeneous dispersed carbon black in the first tape cast, carbon black was pre-mixed with a processing additive specially made for dispersing carbon black, BYK3955 P. A dispersant content of 0,25 wt% was suggested by Dr. Jonas Gurauskis.

Carbon black, BYK 3955 P, EtOH (100%) and ZrO_2-balls (40 balls, Ø10mm) were added to a bottle (PE, 250ml). The specific contents can be seen in Table 3-13. The solution was ball milled (60 rpm, 1h) and further mixed by slow rolling (30 rpm, 24h). The homogenous solution was dried in a rotavapor and dried carbon black mix was collected.

Table 3-13: Contents of carbon black mixed with dispersant

Carbon black mix	
Carbon black (g)	20.000
BYK 3955 P (g)	0.500
EtOH (g)	100

A second tape casting slurry was then prepared. Coarse LSFTa, dispersant (1/10 Darvan-C), distilled water and ZrO_2-balls (3 balls, Ø10mm) were added to a bottle (PE, 125ml). The ceramic particles were stabilized by slow rolling (≈30rpm, 4h)

Pore former (pre-mixed carbon black) and processing additives were added to the slurry and homogenization was achieved by slow rolling (≈30rpm, 24h).

Slurry contents and specified processing additives used can be seen in Table 3-14.

Table 3-14: Contents of second tape casting slurry w/ 32 vol% carbon black as pore former

LSFTa_32CB			
Coarse LSFTa		15.000g	
Pre-mixed carbon black		1.5010g	
Distilled water		3.300g	
Processing additives used			
Darvan-C	0.2 wt% of LSFTa	0.300g	Dispersant
Duramax B1000	15.0 wt% of total powder	2.475g	Binder
Duramax B1235	10.0 wt% of total powder	1.650g	Binder
BYK 3455	0.75 wt% of total slurry contents	0.1817g	Plasticizer

The homogenous slurry was degassed (<40mbar, 10min). Degassed slurry was tape casted into a second tape (height 1000µm, R.T., 60 % speed).

A sample was punched out from the dry tape by a sharp edged steel cylinder (Ø35mm) and sintered according to the heat program shown in Figure 3-8.

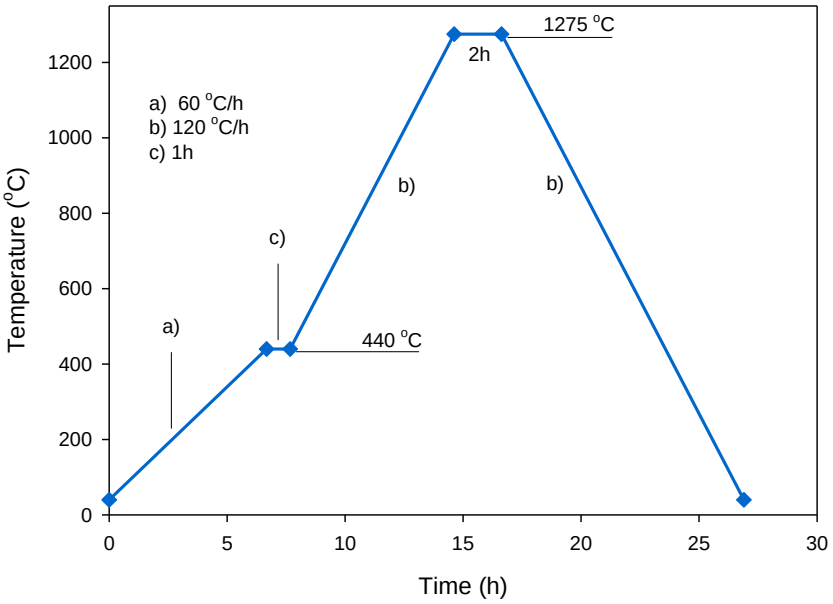

Figure 3-8: Original heat program used for sintering of tape casted samples

Due to an unsuccessful sintering of tape casted sample, a TGA (5 °C/min, max 1000 °C) was carried out and a new sintering program was developed from the TG-results. A second sample was punched out (Ø35mm) and successfully sintered according to the new heat program seen in Figure 3-9.

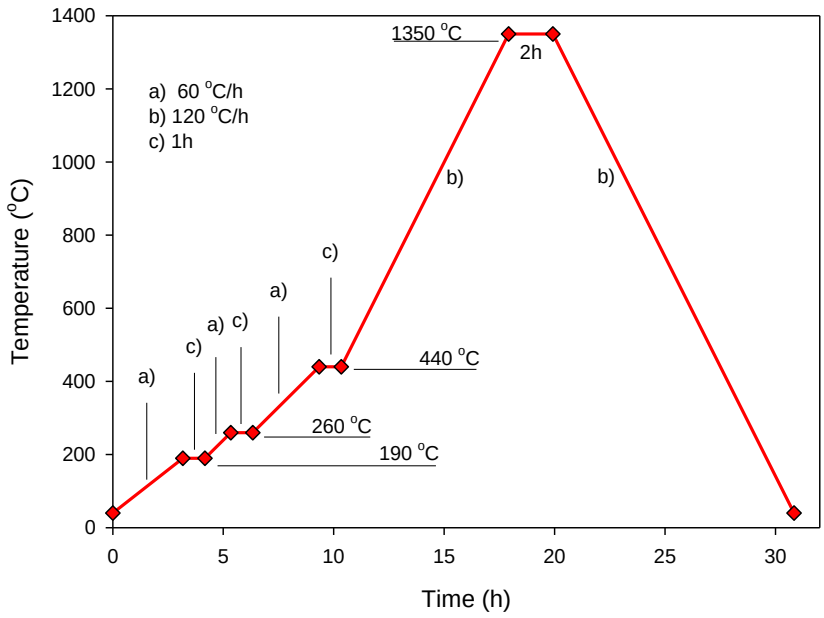

Figure 3-9: New adjusted heat program used for sintering of tape casted samples, with intermediate dwelling temperatures

Tape casting of coarse $La_{0.2}Sr_{0.8}Fe_{0.8}Ta_{0.2}O_{3-\delta}$ and carbon black pore former, with fine $La_{0.2}Sr_{0.8}Fe_{0.8}Ta_{0.2}O_{3-\delta}$ added as sintering aid

A tape casting slurry was made based on previous tape casts, with fine particles added as sintering aid. Coarse LSFTa, fine LSFTa, dispersant (1/10 Darvan-C), distilled water and ZrO_2-balls (3 balls, Ø10mm) were added to a bottle (PE, 125ml). The ceramic particles were stabilized by slow rolling (≈30rpm, 4h)

Pore former (pre-mixed carbon black) and processing additives were added to the slurry and homogenization was achieved by slow rolling (≈30rpm, 24h).

The homogenous slurry was degassed (<40mbar, 10min). Degassed slurry was tape casted (height 1000µm, R.T., 60 % speed).

Slurry contents and specified processing additives used can be seen in Table 3-15.

Table 3-15: Contents of second tape casting slurry w/ 32 vol% carbon black as pore former

LSFTa_32CB_20SA			
Coarse LSFTa		15.000g	
Fine LSFTa		0.144g	
Pre-mixed carbon black		1.519g	
Distilled water		3.333g	
Processing additives used			
Darvan-C	0.2 wt% of LSFTa	0.327g	Dispersant
Duramax B1000	15.0 wt% of total powder	2.4995g	Binder
Duramax B1235	10.0 wt% of total powder	1.6663g	Binder
BYK 3455	0.75 wt% of total slurry contents	0.1837g	Wetting agent

One sample was punched out (Ø35mm) of the tape and sintered according to the heat program shown in Figure 3-9. Structure of successfully sintered substrate was characterized by SEM.

Tape casting of coarse $La_{0.2}Sr_{0.8}Fe_{0.8}Ta_{0.2}O_{3-\delta}$ and cellulose acetate pore former

Tape casting slurry was made based on previous tape casts, but with cellulose acetate acting as pore former instead of carbon black. Coarse LSFTa, dispersant (1/10 Darvan-C), distilled water and ZrO_2-balls (3 balls, Ø10mm) were added to a bottle (PE, 125ml). The ceramic particles were stabilized by slow rolling (≈30rpm, 4h)

Pore former (cellulose acetate) and processing additives were added to the bottle and homogenization was achieved by slow rolling (≈30rpm, 24h).

The homogenous slurry was degassed (<40mbar, 10min). Degassed slurry was tape casted (height 1000µm, R.T., 60 % speed).

Slurry contents and specified processing additives used can be seen in Table 3-16.

Table 3-16: Contents of second tape casting slurry w/ 32 vol% cellulose acetate as pore former

LSFTa_32CA			
Coarse LSFTa		15.000g	
Cellulose acetate		1.000g	
Distilled water		3.300g	
Processing additives used			
Darvan-C	0.2 wt% of LSFTa	0.300g	Dispersant
Duramax B1000	15.0 wt% of total powder	2.400g	Binder
Duramax B1235	10.0 wt% of total powder	1.600g	Binder
BYK 3455	7.5 wt% of total slurry contents	1.770g	Plasticizer

One sample was punched out (Ø35mm) of the tape and sintered according to the heat program shown in Figure 3-9. Structure of sintered sample was characterized by SEM.

3.2.9 Mechanical properties of tape casted porous substrates

Fracture load of porous substrates made by tape casting was measured using Instron 5543. Only the porous substrates made by carbon black pore former were successfully sintered, as the cellulose acetate substrate warped during heating. The biaxial strength was calculated from fracture load and substrate geometry according to Eq.2.20.

After mechanical testing, three samples of the most promising tape cast were sintered according to Figure 3-9. The porosity was measured by the previously explained Archimedes method and permeability of the substrates was measured using the RDC-145.

4 Results

4.1 Characterization of $La_{0.2}Sr_{0.8}Fe_{0.8}Ta_{0.2}O_{3-\delta}$

Solid state powder synthesized at 1300 °C was analyzed by XRD. The XRD-spectra of solid state powder shows that the powder is a single phase LSFTa-perovskite powder and the spectra can be seen in Figure 4-1.

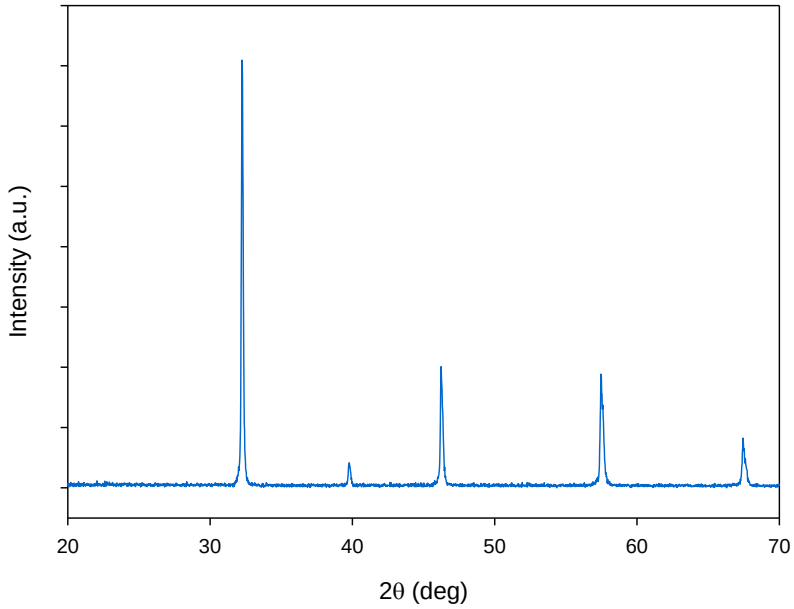

Figure 4-1: XRD-spectra of solid state powder synthesized at 1300 °C showing a single phase $La_{0.2}Sr_{0.8}Fe_{0.8}Ta_{0.2}O_{3-\delta}$-perovskite

Particle size distribution of the solid state powder was characterized by laser diffraction technique and SEM was used to image the morphology of the powder. The particle size distribution of the solid state LSFTa is shown in Figure 4-2.

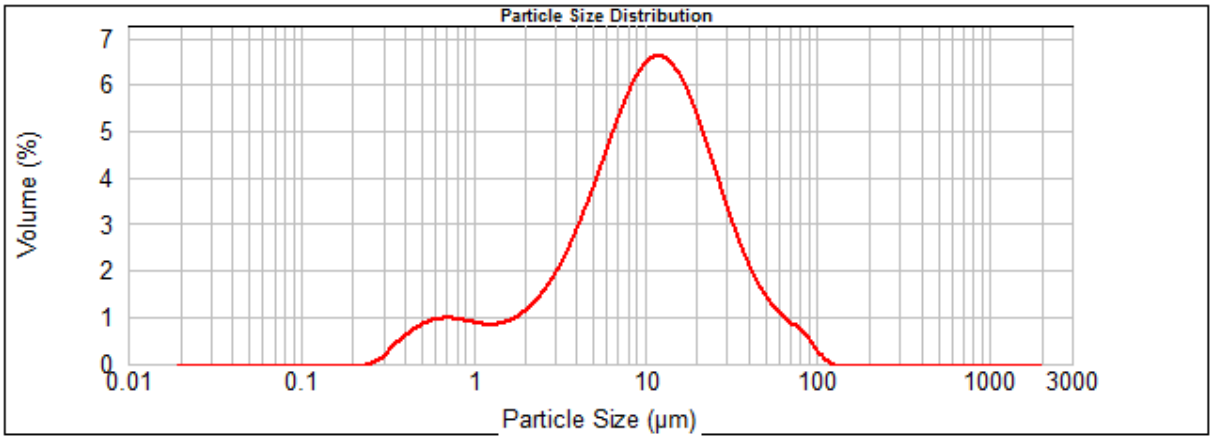

Figure 4-2: Particle size distribution of the solid state LSFTa showing a main constituent particle size around 10µm, with extreme sized particles ranging up to 100µm

The particle size distribution analysis shows that the main constituent particle size of the powder is around 10µm, while some extreme sized particles range up to around 100µm. Figure 4-2 also shows that the solid state batch also contains a small amount of particles which range down to sub-micron size. A SEM-image of the coarse LSFTa-powder can be seen in Figure 4-3a. Imaged particles can be seen to correlate well with the particle size distribution analysis, as most particles in the image range between 10-50µm, and are covered by a number of sub-micron particles.

Fine powder synthesized by spray pyrolysis was also imaged by SEM and its particle size was estimated by BET-analysis. The SEM-image in Figure 4-3b is unable to show a specific particle size, but it is clear that the particle size distribution is sub-micron for the spray pyrolysed powder.

BET surface area was measured to 11.3494m^2/g for the spray pyrolysed powder. Assuming homogeneously sized spherical particles, the average particle size of the spray pyrolysed powder can be estimated by the theoretical density of 6.3g/cm^3. The BET surface area then corresponds to an average particle size of ≈85nm for the spray pyrolysed powder, which should have a large effect on the sintering behavior of the fine powder compared to that of coarse LSFTa from solid state reaction.

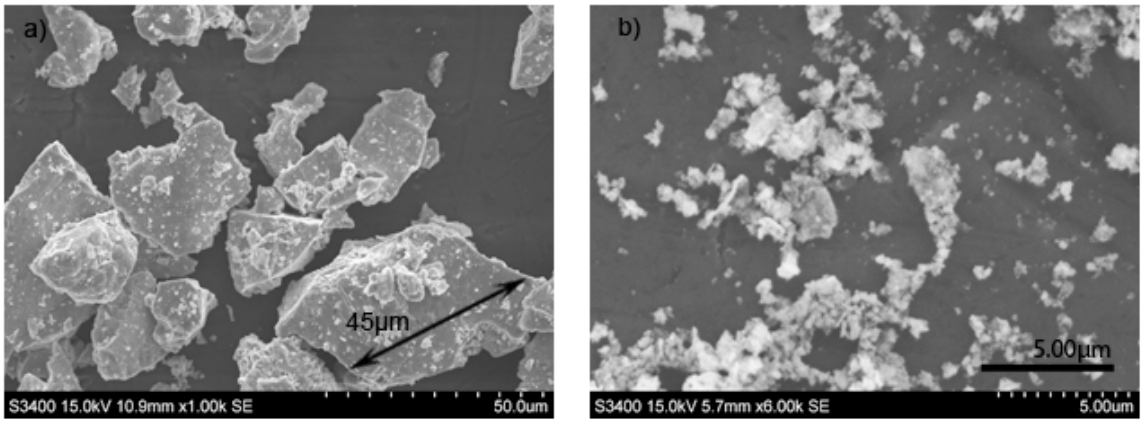

Figure 4-3: a) Coarse LSFTa-powder synthesized by solid state reaction at 1300 °C, showing particles ranging from sub-micron and up to ≈50µm, x1000 magnification b) Fine LSFTa synthesized by spray pyrolysis, calcined at 800 °C, x6000 magnification

DIL-analysis was used to characterize the sintering behavior of the two different powders. Results from DIL-analysis can be seen in Figure 4-4. The sintering temperatures of the two different powders are well separated, and a sintering temperature of 1200 °C will mainly affect the spray pyrolysed powder.

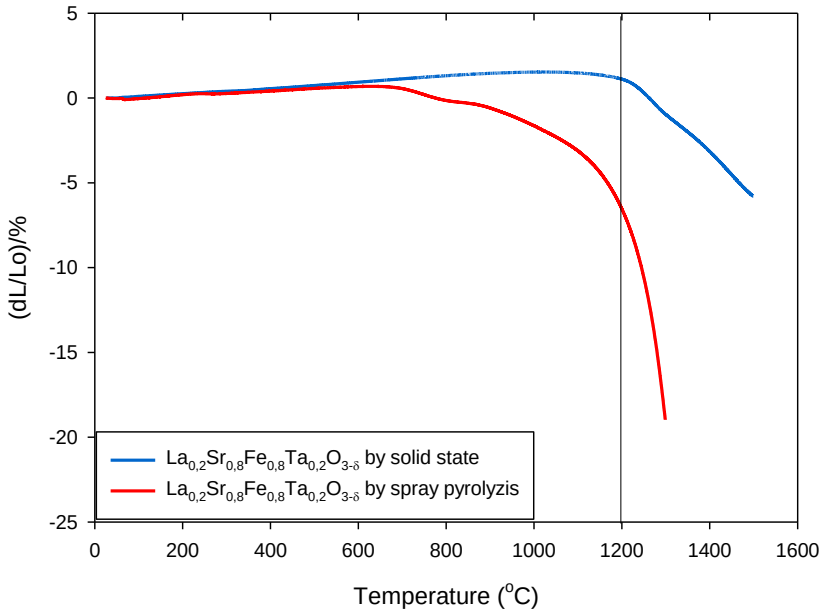

Figure 4-4: Dilatomer analysis of solid state and spray pyrolysed powder showing contraction of sample (in %) as a function of temperature, showing the difference in sintering behavior of the two powders

4.2 Characterization of pore formers

SEM-images of the two pore formers can be seen in Figure 4-5a and Figure 4-5b. The carbon black seen in Figure 4-5a are elongated, variable sized rods ranging from a few micron and up to 200µm long. In comparison the cellulose acetate seen in Figure 4-5b are more spherical shaped particles, mainly ranging between 100 and 300µm.

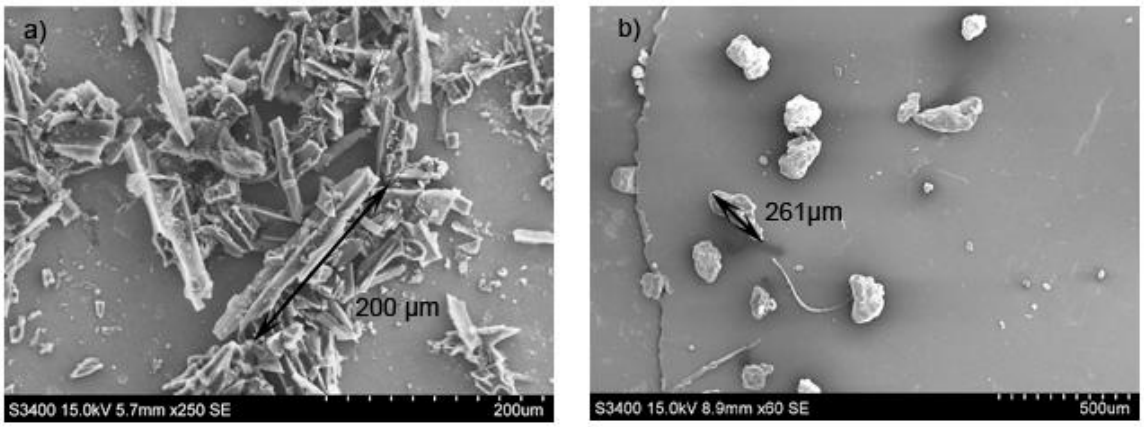

Figure 4-5: a) Carbon black pore former seen as elongated, variable sized rods ranging up to 200µm length, x250 magnification b) More spherical shaped cellulose acetate pore former ranging between 100-300µm in size, x60 magnification

Ash contents of the two pore formers were measured by firing two small samples and estimated to ≈0.73 % for carbon black, compared to a low <0.1% for cellulose acetate. Weight measurements and calculations of ash contents can be found in appendix E.

4.3 Investigating optimum amount of dispersant

Viscosity as a function of wt% Darvan-C of four different samples (0.2 – 0.6 wt% Darvan-C) is shown in Figure 4-6, measured by HAAKE Mars III.

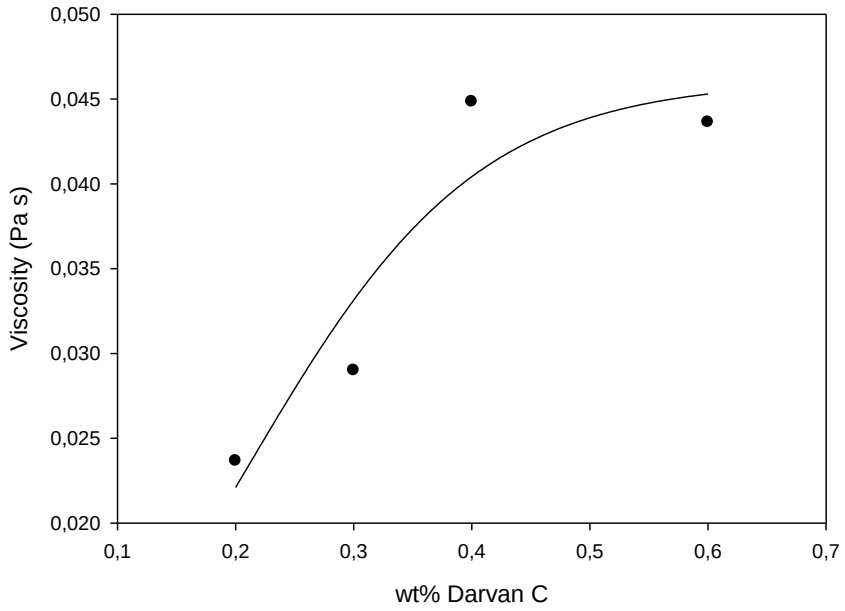

Figure 4-6: Viscosity as a function of wt% Darvan-C for solid state $La_{0.2}Sr_{0.8}Fe_{0.8}Ta_{0.2}O_{3-\delta}$ in water solute, showing full coverage of Darvan-C at 0.2 wt%

The amount of Darvan-C needed to obtain full coverage of particles, resulting in the stable slurry needed for tape casting, was found to be 0.2 wt% of coarse powder. The increase in viscosity indicates that full coverage of particles is achieved.

The surface area of the coarse powder was measured to 0.5368m^2/g. Literature on similar powders estimated an optimum amount of 0.31 mg/m^2, which corresponds to 0.23 wt% for the solid state LSFTa.

4.4 Producing pressed porous substrates

4.4.1 Coarse $La_{0.2}Sr_{0.8}Fe_{0.8}Ta_{0.2}O_{3-\delta}$ with fine particles of $La_{0.2}Sr_{0.8}Fe_{0.8}Ta_{0.2}O_{3-\delta}$ added as sintering aid

SEM-images of three pressed pellets made from combinations of coarse and fine powder, without pore former, can be seen in Figure 4-7a, b and c. The pellets were successfully sintered at 1200 °C, but the SEM-images are indicating a poor structure with respect to permeability, with a high degree of tortuosity in the sintered substrate.

Apparent porosity of samples made from coarse and fine powder was measured using the previously mentioned Archimedes method. Apparent porosity was found to be 27% for all samples. Due to the apparent poor permeating structure, the substrates without pore formers were not tape casted.

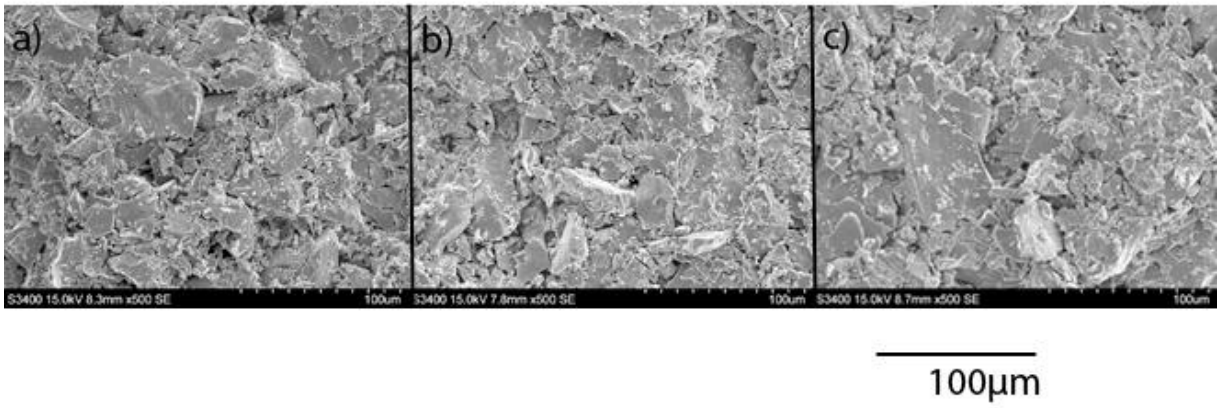

Figure 4-7: Fracture surface of the three pressed pellets, x500 magnification a) LSFTa_05SA b) LSFTa_10SA c) LSFTa_20SA

4.4.2 Coarse $La_{0.2}Sr_{0.8}Fe_{0.8}Ta_{0.2}O_{3-\delta}$ with carbon black pore former

Pressed porous substrates made from coarse LSFTa with 32 vol% carbon black pore former were successfully sintered at both 1275 °C and 1350 °C. SEM-images showing the fracture surface of these pellets can be seen in Figure 4-8a and Figure 4-8b. Both substrates are showing good connected porosity for gas permeability. The apparent porosity was measured by Archimedes method and found to be 41 % and 22 % for substrates sintered at 1275 °C and 1350 °C respectively.

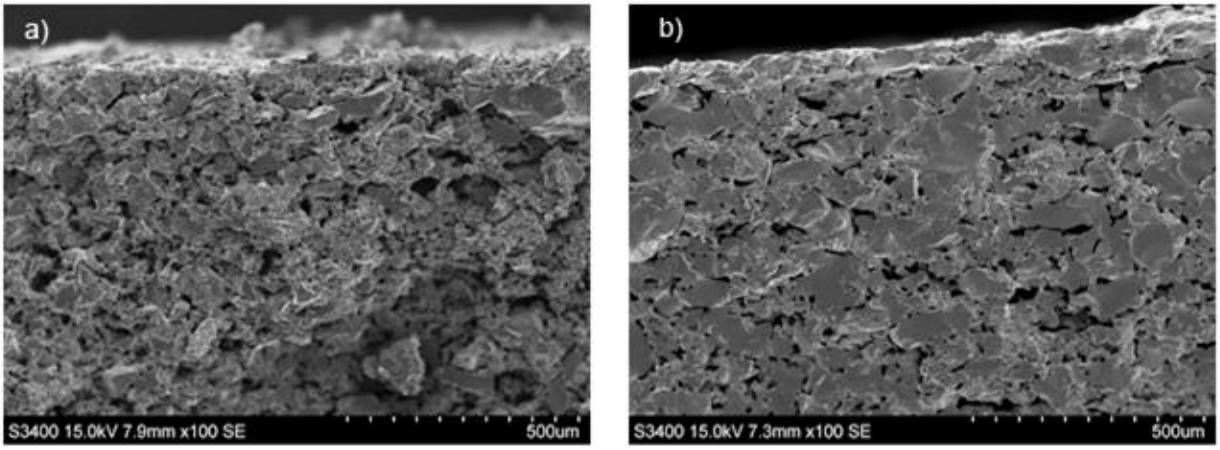

Figure 4-8 : Fracture surface of pressed LSFTa_32CB at x100 magnification
a) Sintered at 1275 °C, 41 % apparent porosity b) Sintered at 1350 °C, 22 % apparent porosity

4.4.3 Coarse $La_{0.2}Sr_{0.8}Fe_{0.8}Ta_{0.2}O_{3-\delta}$ and carbon black pore former, with fine $La_{0.2}Sr_{0.8}Fe_{0.8}Ta_{0.2}O_{3-\delta}$ added as sintering aid

Pressed porous substrates made from coarse LSFTa and carbon black pore former, with fine particles added as sintering aid, were successfully sintered at both 1275 °C and 1350 °C. SEM-images showing the fracture surface of these pellets can be seen in Figure 4-9a and Figure 4-9b. Both substrates are showing good connected porosity for gas permeability.

The apparent porosity was measured by Archimedes method and found to be 39 % and 20 % for substrates sintered at 1275 °C and 1350 °C respectively. The substrate sintered at 1350 °C is showing a higher degree of necking and more rounded particles, indicating the higher degree of sintering compared to that of the substrate sintered at 1275 °C.

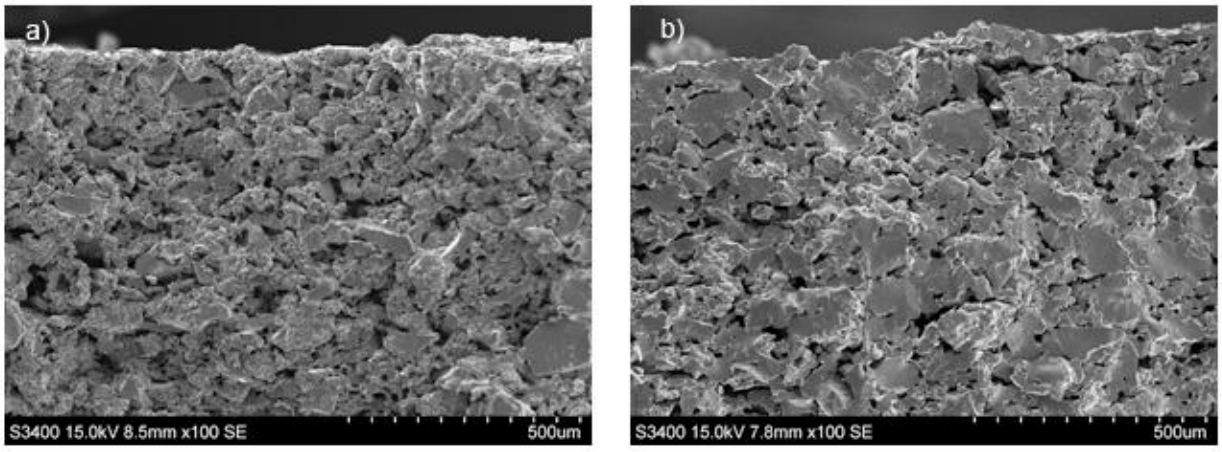

Figure 4-9: Fracture surface of pressed LSFTa_32CB_20SA at x100 magnification
a) Sintered at 1275 °C, 39 % apparent porosity b) Sintered at 1350 °C, 20 % apparent porosity

4.4.4 Coarse $La_{0.2}Sr_{0.8}Fe_{0.8}Ta_{0.2}O_{3-\delta}$ with cellulose acetate pore former

Pressed porous substrates made from coarse LSFTa with cellulose acetate pore former were successfully sintered at 1275 °C and 1350 °C. SEM-images showing the fracture surface of these pellets can be seen in Figure 4-10a and Figure 4-10b. The open porosity was measured by Archimedes method and found to be 27 % for both samples.

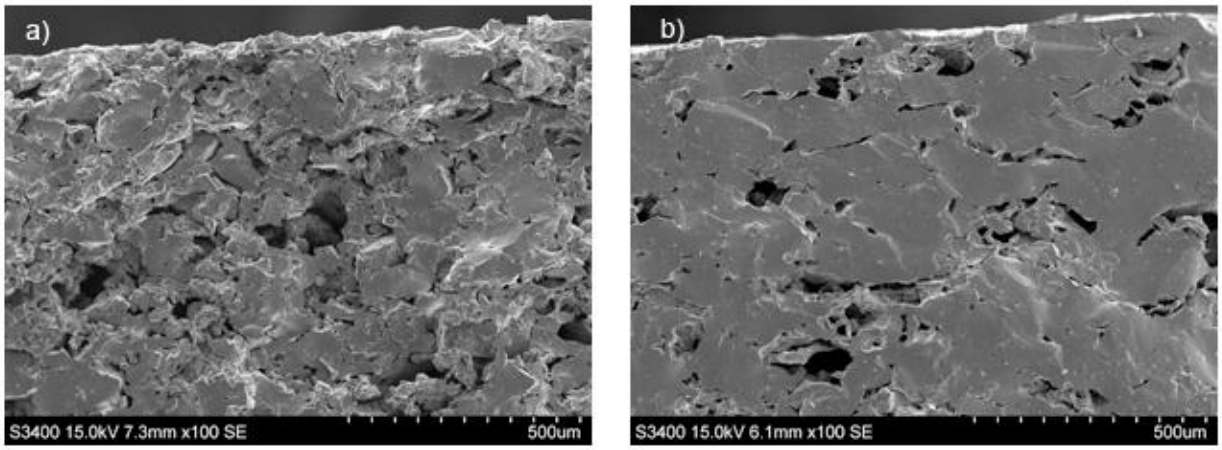

Figure 4-10: Fracture surface of pressed LSFTa_32CA at x100 magnification
a) Sintered at 1275 °C, 27 % apparent porosity b) Sintered at 1350 °C, 27 % apparent porosity

4.5 Permeability of pressed porous substrates

The permeability of the porous substrates calculated by the RDC-145 needed to be adjusted to the actual test geometry in the modified sample holder according to Eq. 2.10. Permeability measurements before adjustments, geometry factors and adjustment calculation can be seen in

appendix D. The actual permeability of the different samples and their apparent porosity can be seen in Table 4-1.

Table 4-1: Permeability (nPm) and apparent porosity (%) of pressed porous substrates of three different compositions, sintered at 1275 °C and 1350 °C respectively

Substrate Sample	Permeability (nPm)	Apparent porosity (%)
Sintered at 1275 °C		
LSFTa_32_CB	29,1	41
LSFTa_32_CB_20SA	27,5	39
LSFTa_32_CA	15,7	27
Sintered at 1350 °C		
LSFTa_32_CB	11,5	22
LSFTa_32_CB_20SA	8,3	20
LSFTa_32_CA	9,1	27

Permeability related to the sintering temperature of the different substrates from Table 4-1 can be seen plotted in Figure 4-11.

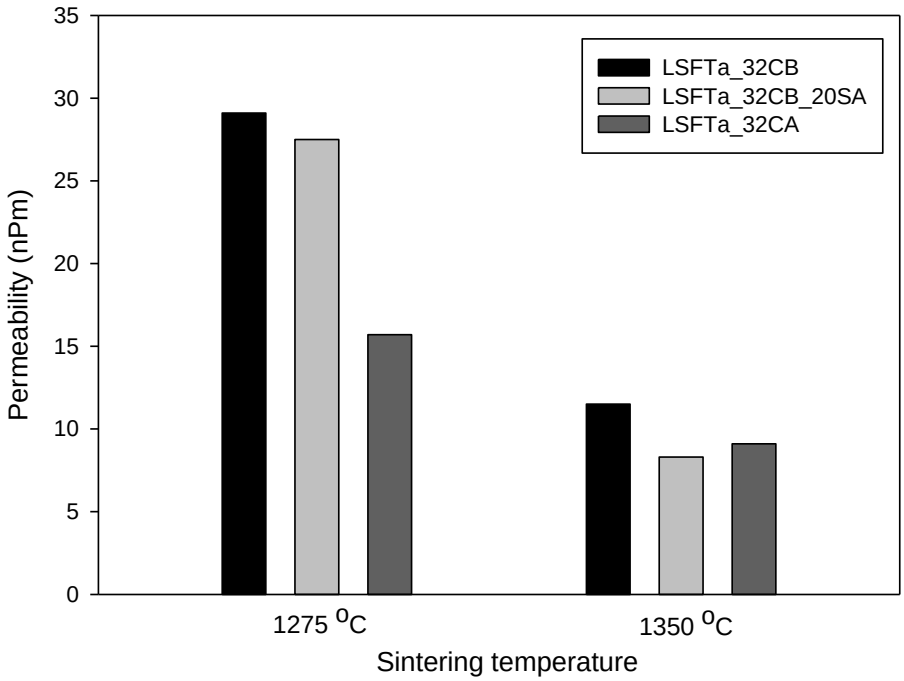

Figure 4-11: Permeability(nPm) of the three different powder compositions as pressed substrates, sintered at 1275 °C and 1350 °C respectively

4.6 Tape casting of porous substrates

4.6.1 Coarse $La_{0.2}Sr_{0.8}Fe_{0.8}Ta_{0.2}O_{3-\delta}$ with carbon black pore former

Images of the first tape cast with 32 vol% carbon black is shown in Figure 4-12, with a close up image showing the inhomogeneously dispersed carbon black.

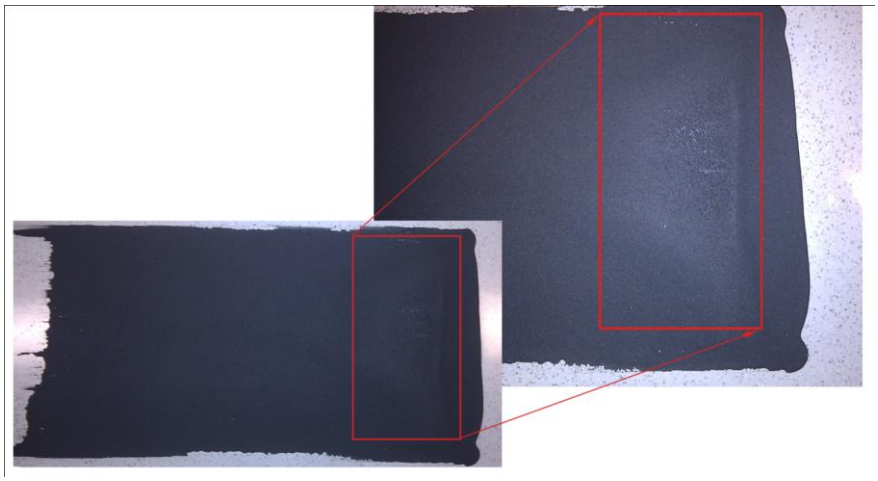

Figure 4-12: Image showing LSFTa_32CB tape cast with inhomogeneously dispersed carbon black

Due to trouble dispersing carbon black, the carbon black was pre-mixed with BYK 3955 P. A successful tape cast with pre-mixed carbon black was then performed. The first sintering of the green bodies using the original heat program, as shown earlier in Figure 3-8, resulted in broken and disfigured substrates. The remains of these substrates can be seen in Figure 4-13.

Figure 4-13: Remains of two broken and disfigured LSFTa_32CB-substrates

TGA of tape casted sample was therefore carried out to set a new heat program. Results from TGA can be seen in Figure 4-14, where the mass% of the original sample is plotted as a function of increasing temperature. The burnout temperatures of the different processing

additives can be found as the mass of the sample decreases with increasing temperature. A rapid loss of mass can be seen at temperatures of about 200, 270 and 450 °C.

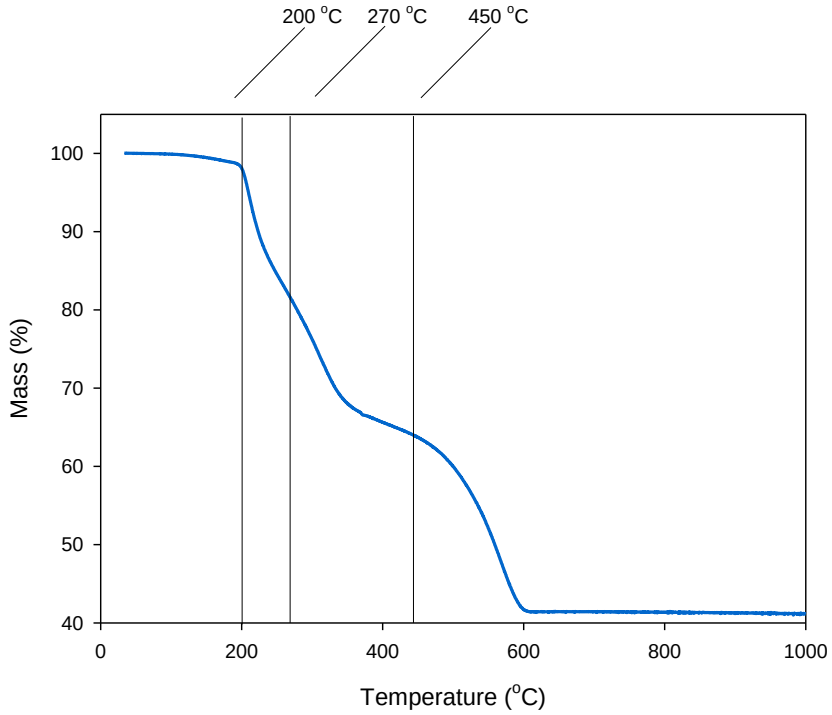

Figure 4-14: Thermal gravimetric analysis of tape casted LSFTa_32CB showing remaining mass (in %) as a function of temperature. Rapid loss of mass can be seen at temperatures of about 200, 270 and 450 °C

The first derivative of the TGA further enhances the loss of mass in the sample. TGA was used to tailor the sintering program according to the burn-off temperatures of the additives used. The first derivative of the TGA in Figure 4-14, and the intermediate dwelling temperatures added in the sintering program as a result of this analysis, can be seen in Figure 4-15.

The adjusted heat program resulted in a successful sintering of tape casted substrates. However, as the pressed substrate sintered at 1275 °C proved very fragile upon handling, the maximum sintering temperature was increased to 1350 °C.

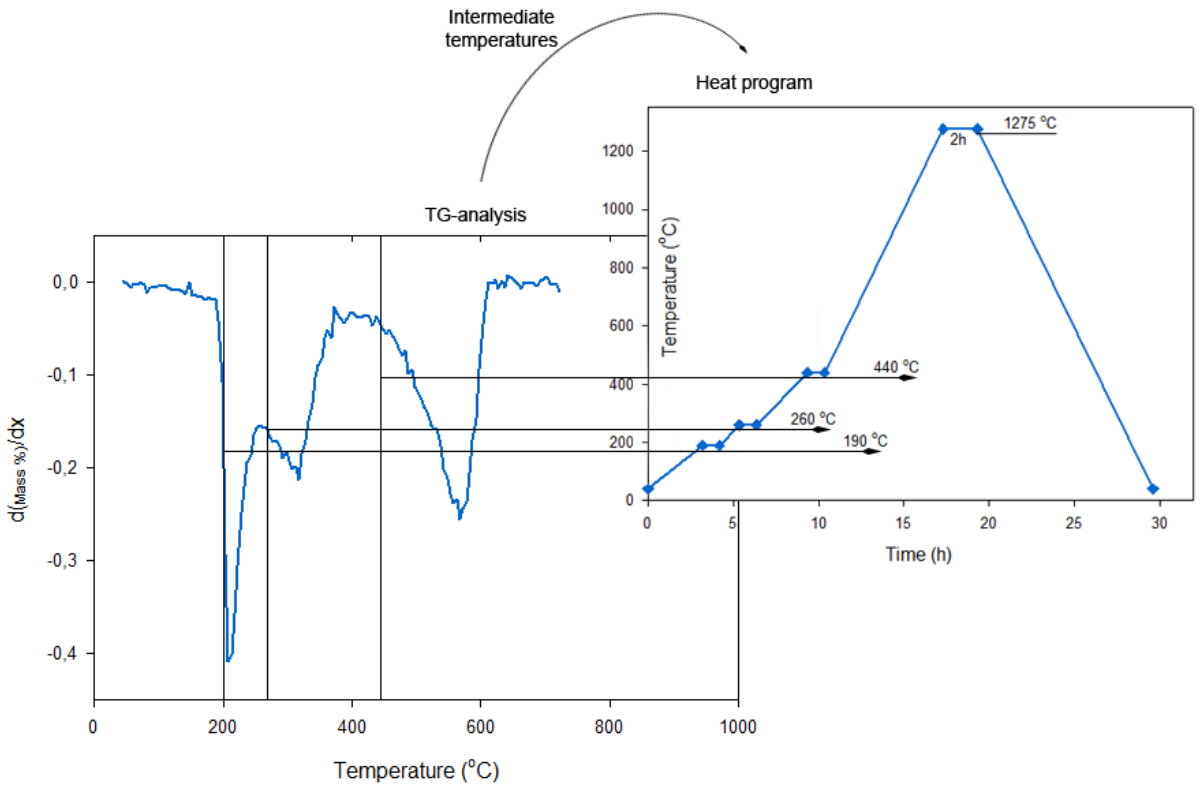

Figure 4-15: First derivative of Figure 4-14 (to the left), and how the analysis is used to add intermediate dwelling temperatures in sintering program (to the right) to avoid warping due to rapid loss of mass during heating

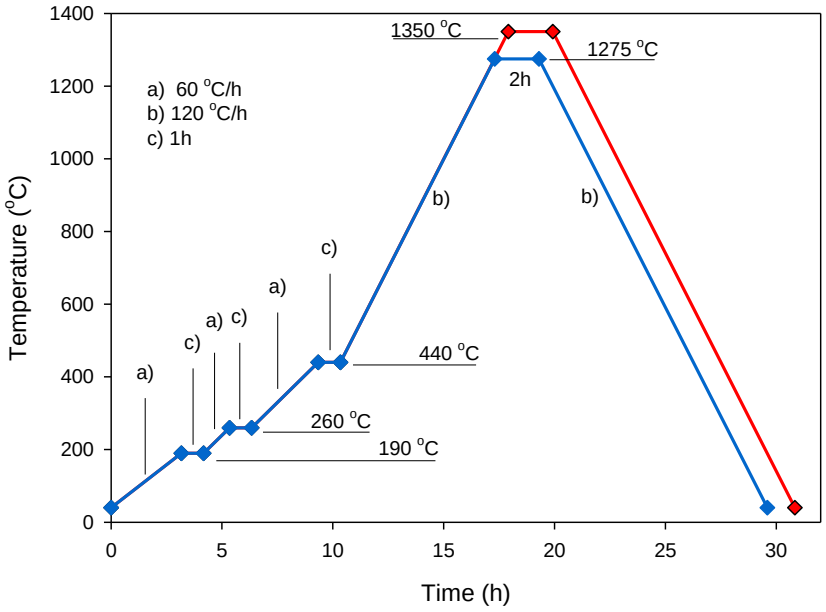

Figure 4-16: Final heat program for LSFTa_32CB and LSFTa_32CB _20SA and LSFTa_32CA, with intermediate heating steps and increased sintering temperature

SEM-images showing the fracture surface of the tape casted porous substrate sintered at 1350 °C can be seen in Figure 4-17a and Figure 4-17b. It shows good connected porosity in a 361µm thick substrate.

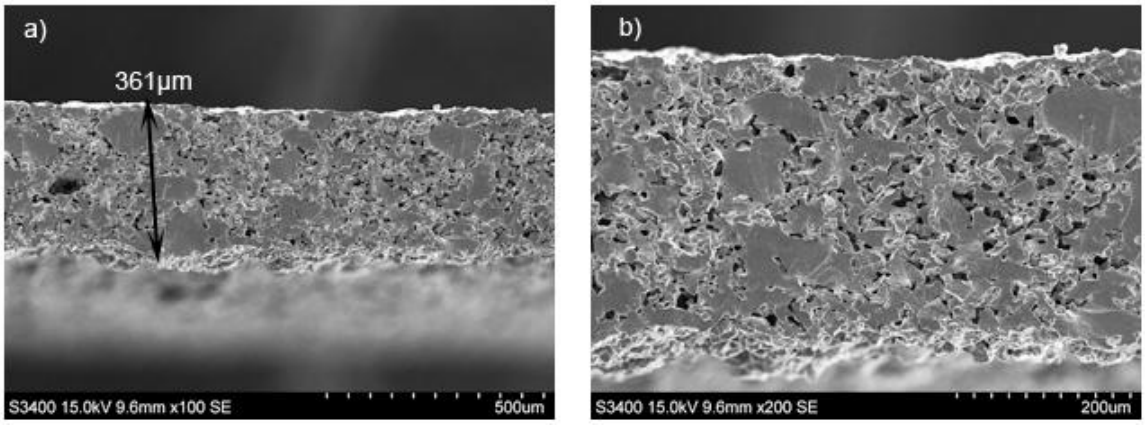

Figure 4-17: Fracture surface of tape casted LSFTa_32CB
a) x100 magnification, with a measured thickness of 361µm b) x200 magnification

4.6.2 Coarse $La_{0.2}Sr_{0.8}Fe_{0.8}Ta_{0.2}O_{3-\delta}$ with carbon black pore former, with fine particles of $La_{0.2}Sr_{0.8}Fe_{0.8}Ta_{0.2}O_{3-\delta}$ added as sintering aid

A substrate consisting of coarse LSFTa and carbon black pore former, added fine sized particles of LSFTa as sintering aid, was successfully sintered at 1350 °C according to the heat program seen in Figure 4-16. SEM-images showing the fracture surface of the porous substrate can be seen in Figure 4-18a and Figure 4-18b. The substrate shows good connected porosity in a 391µm thick substrate. The pores are smaller and more homogeneously dispersed compared to that of the same substrate without the added fine particles.

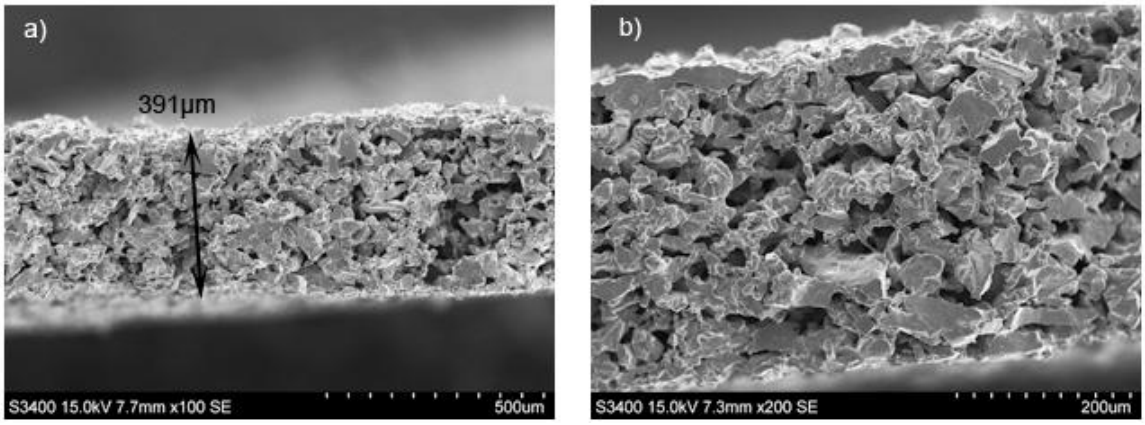

Figure 4-18: Fracture surface of tape casted LSFTa_32CB_20SA
a) x100 magnification, with a measured thickness of 391µm b) x200 magnification

4.6.3 Coarse $La_{0.2}Sr_{0.8}Fe_{0.8}Ta_{0.2}O_{3-\delta}$ with cellulose acetate pore former

TGA of tape casted sample containing cellulose acetate was performed (5 °C/min, max 1000 °C) to set the sintering program for the new pore former. Results from TGA of the tape casted sample can be seen in Figure 4-19, where mass% of the original sample is plotted as a function of increasing temperature. A continuous loss of mass can be seen between temperatures of about 190 °C and 370 °C. The sintering programs presented earlier in Figure 3-5, Figure 3-6 and Figure 3-9 for substrates containing cellulose acetate was based on this analysis.

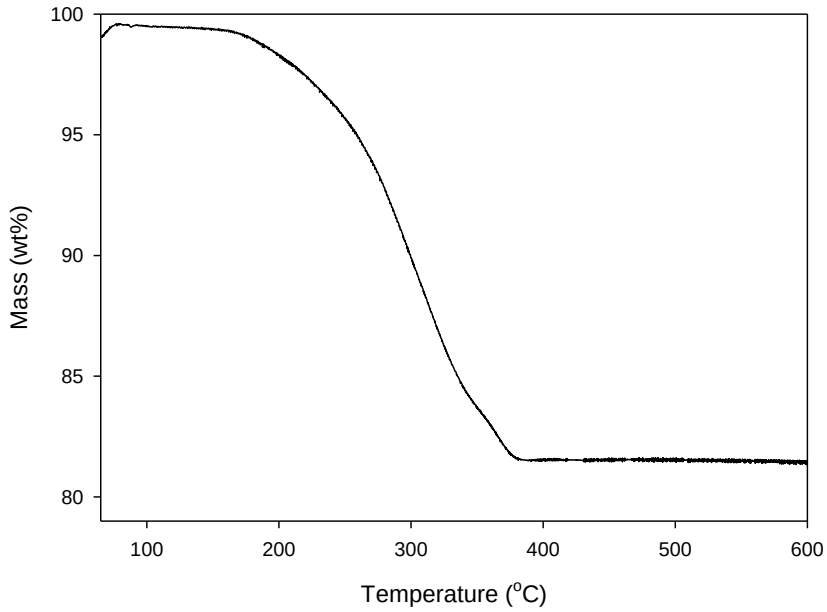

Figure 4-19: TGA of tape casted LSFTa and cellulose acetate pore former, showing sample mass (in %) as a function of increasing temperature. A large loss of mass can be seen at temperatures between 190 °C and 370 °C

A substrate with cellulose acetate pore former was sintered at 1350 °C according to Figure 4-16. SEM-images showing the fracture surface of the substrate is shown in Figure 4-20a and Figure 4-20b. The substrate was not successfully sintered, as it warped and deformed during heating. The inhomogeneous structure seen in Figure 4-20a and Figure 4-20b points towards a poor homogenization.

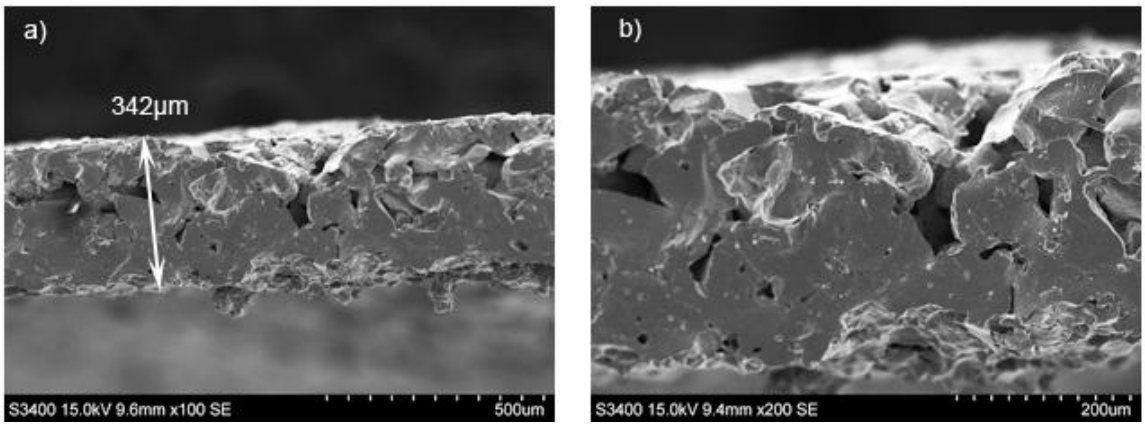

Figure 4-20: Fracture surface of tape casted LSFTa_32CA
a) x100 magnification, with a measured thickness of 342µm b) x200 magnification

4.7 Biaxial strength of tape casted substrates

The fracture load of the porous substrates was measured by ball-on-ring test, and strength was calculated from fracture load according to Eq. 2.20. As the cellulose acetate containing substrate warped during sintering, strength measurement of this substrate was not possible. The measured strength of the carbon black containing substrates are shown in Table 4-2 and plotted in Figure 4-21.

$$S = \frac{3 \cdot F_N \cdot (1+v)}{4 \cdot \pi \cdot t^2}\left[1 + 2\ln\left(\frac{a}{b}\right) + \left(\frac{1-v}{1+v}\right)\left(\frac{a}{R}\right)^2\left(1 - \left(\frac{b^2}{2a^2}\right)\right)\right] \qquad (2.20)$$

Table 4-2: Measured strength of porous substrates made by tape casting

Substrate sample	Biaxial strength (MPa)
LSFTa_32CB	37.4
LSFTa_32CB_20SA	34.2
LSFTa_32CA	-

Measured strength of both carbon black tape casts indicates that the substrates are able to match the mechanical strength of similar porous substrates.

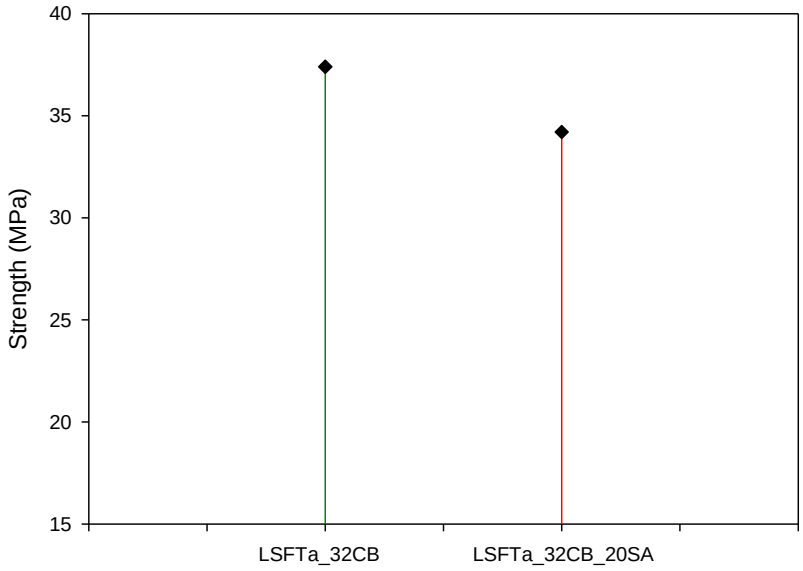

Figure 4-21: Measured strength of tape casted porous substrates.

4.8 Permeability of tape casted substrates

The LSFTa_32CB-substrate measured the highest strength of 37.4MPa and three more samples were therefore successfully sintered at 1350 °C according to Figure 4-16. Porosities of three substrates were measured to an average of 28%. An average air permeability of the tape casted LSFTa_32CB, compared to the previously measured pressed substrates also sintered at 1350 °C, is shown in Figure 4-22.

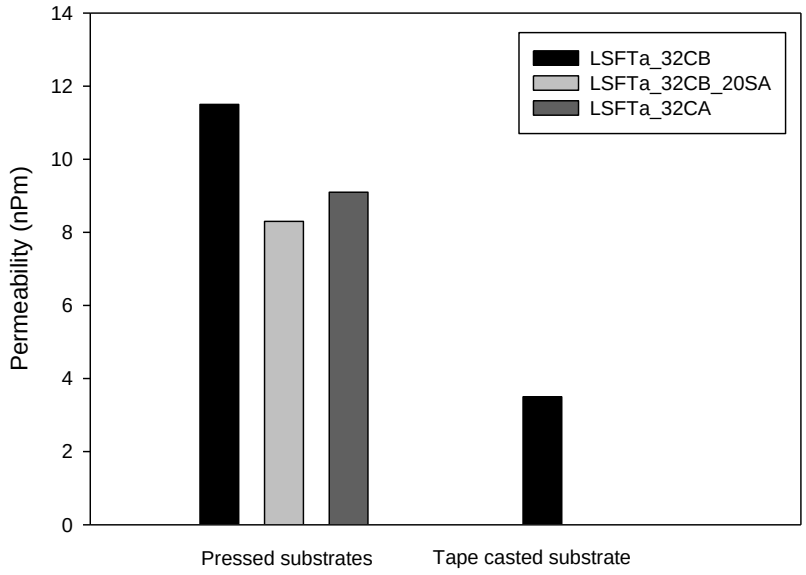

Figure 4-22: Permeability of tape casted LSFTa_32CB compared to pressed substrates

The permeability of the tape casted LSFTa_32CB is significantly lower than the previously made pressed LSFTa_32CB-substrate, even though its apparent porosity is higher than the pressed pellets.

5 Discussion

5.1 Characterization of $La_{0.2}Sr_{0.8}Fe_{0.8}Ta_{0.2}O_{3-\delta}$

$La_{0.2}Sr_{0.8}Fe_{0.8}Ta_{0.2}O_{3-\delta}$ was successfully synthesized by solid state reaction. XRD-spectra confirm a single phase powder. Particle size distribution analysis by laser diffraction technique shows a main constituent particle size around 10µm, while particle size distribution varies from sub-micron to 100µm. This particle size distribution is confirmed by SEM-imaging.

Estimating average particle size from BET-surface area results in 1,8µm for the solid state powder. This is a bit off from laser diffraction technique and SEM-analysis results, but estimating particle size from BET also assumes homogenous sized spherical particles, which is far from the case concerning this powder. Spray pyrolyzed powder results in a very narrow particle size distribution, and estimating an average particle size of 85nm from BET is therefore assumed to be a good indication of its particle size.

The particle size's effect on the sintering behavior can be seen from the dilatometer analysis in Figure 4-4. The spray pyrolysed sample contracts at a much lower temperature and at a much higher rate compared to that of the coarse powder.

The original sintering temperature of 1275 °C was selected from previous work [33]. As the solid state powder used in this current work is coarser than the powder used in previous work, the sintering driving force had to be increased by increasing the sintering temperature to 1350 °C in order to obtain substrates strong enough to be analyzed.

5.2 Investigating optimum amount of dispersant

Optimum amount of dispersant was found to be 0.2 wt% of coarse powder. This was determined by testing a range between 0.2 - 0.6 wt% dispersant. Test range was based on the value of 0.31mg/m^2 suggested in literature review. Based on the BET-surface area analysis of 0.5368m^2/g for solid state powder, using 0.2 wt% dispersant corresponds to a value of 27mg/m^2.

As 0.2 wt% was the lowest dispersant content in the test range, there is some uncertainty around the statement that this is in fact the minimum viscosity caused by stabilizing the suspension. However, the drastic increase in viscosity as wt% Darvan-C increases above

0.2 wt%, indicates that a full degree of coverage is already achieved at 0.2 wt% and that adding more dispersant will most likely only lead to excess polymer in the suspension. Also, the softening curvature of the viscosity measurements in Figure 4-6 indicates a stabilization of viscosity around this specific amount. Any more specific determination of optimum amount of dispersant is probably possible, but considered irrelevant as stabilization is achieved.

As the solid state synthesis involves manual crushing, the surface area of the produced powder will vary some from batch to batch and the optimum amount of dispersant needs to be adjusted accordingly. For solid state LSFTa the optimum amount can probably be scaled according to the value of $27 mg/m^2$, which was found to be optimum for this batch.

5.3 Producing pressed porous substrates

The different compositions used for the three pressed porous substrates were all mixed with EtOH in small sample glass. The mixing of these was performed by manually shaking them for 5 minutes. This mixing method is different from that done in previous work [13, 33], where the mixing was achieved by ball milling for 30 minutes. Mixing by shaking in a small sample glass was chosen in an attempt to avoid excess damage to the elongated carbon black rods, from the impacts received by the rotating balls in ball mill.

The mixing method does however raise a question of homogenization. As these substrates are intended for permeability measurements and to give a quick indication on structure, it is the distribution of pore formers which is most critical in the mixing process. From the SEM-images of the pressed porous substrates, the porous structure seem homogeneously dispersed, and there is no indication of that the small degree of variation in structure is nothing more than the result of the heterogeneous morphology of the pore formers. Therefore, the substrates are believed to be sufficiently homogenously dispersed to serve their use as structural indicators and for permeability measurements.

5.4 Porosity porous substrates

Porosity measurements were carried out by Archimedes method using iso-propanol. This is a liquid which evaporates quickly, and care must be taken during analysis to achieve correct results. Evaporation of iso-propanol might be a source of error for these measurements. Measuring porosity of cracked or damaged samples will lead to severe error in the analysis.

The permeability results are measured using a modified sample holder. The modified sample holder's double constricting layer consisting of steel and rubber is assumed to sufficiently seal the substrate. Two layers consisting of steel and rubber on each side of the substrate, limits the air flow on the substrate to a circular area (Ø1cm). A homogenous substrate is therefore assumed. Any inhomogenities in the structures might alter the measured permeability.

5.4.1 Effect of powder particle size distribution

The substrates sintered at 1275 °C achieved porosities ranging up to 41 % and also reached the highest permeabilities. However, as some of the substrates sintered at 1275 °C were lacking sufficient mechanical strength to be tested, only the substrates sintered at 1350 °C are considered realistic with respect to permeation.

The porous substrates made with fine particles as sintering achieved an apparent porosity of 20 % when sintered at 1350 °C. This is 2 % below the porosity obtained by the same substrates produced without the fine particles, and might be an effect from the increased sintering characteristics of the added fine particles have in the substrate. When mixing particles of varying size, it is theoretically possible to achieve a higher degree of packing, which might have affected the porosity.

5.4.2 Effect of pore former morphology

Carbon black can be seen in Figure 4-5 to be elongated rods of varying length. The rods range up to 200µm, but as the powder is very fragile many of the rods seem to be easily broken and crushed. Care must therefore be taken during processing, in order to maintain the elongated rod shapes of the carbon black. This makes it challenging to estimate a specific size of the carbon black in the final green body.

The cellulose acetate is more spherical compared to the carbon black. This results in a very different pore formation as can be seen from Figure 4-8 and Figure 4-10. Its particle size estimated by SEM indicates a size range between 150-300µm. The morphology is without any specific orientation, and the particles are probably not as vulnerable to impacts during processing, compared to that of carbon black.

It is evident that the pore structure from the two pore formers reacts differently to the increased sintering temperature. The apparent porosities of carbon black substrates decreased by about 50 % with the increased sintering temperature, while the cellulose acetate substrate maintained its apparent porosity. However, the SEM-images of the two cellulose acetate substrates in Figure 4-10, indicates that it is very unlikely that the porosity of the two substrates truly are the same. The porosity of the substrates sintered at 1275 °C is therefore assumed to be affected by loss of immersed liquid before weight measurement m_3, and not a subject to further discussion.

5.5 Permeability and flux of pressed porous substrates

All porous substrates made with pore formers achieved permeabilities between 8,3 and 11,5nPm. Highest previously achieved permeability of $La_{0.2}Sr_{0.8}Fe_{0.8}Ta_{0.2}O_{3-\delta}$ has been reported to 1,3nPm [13, 33] where the substrates have been made from relatively fine powders.

This drastic increase in permeability can be explained by the large particle size of the powder used in this work. Assume a specific mass of pore former with a specific volume. A fine sized ceramic powder will allow for a fine distribution of pore former, and hence a fine distribution of final pores. As the substrate sinters, the fine sized pores have a higher chance of shrinking and increasing the degree of tortuosity. The large particles in the solid state powder will limit the pore formers distribution by their large volume, and force the pore former to form wider pores. The wide pores have a higher chance of resisting the shrinkage and the closing of pores during sintering, and in turn ease the viscous flow of gas through the substrate in the final product.

Carbon black containing substrates sintered at 1350 °C are showing a high permeability with regard to their apparent porosity of 22 % and 20 %. The cellulose acetate containing substrate has an apparent porosity of 27 %, and as a consequence this would be expected to result in the better permeability. It is however, still below the best carbon black substrate with respect to permeability. This might indicate that the porous structure made by the cellulose acetate pore former results in a higher degree of tortuosity, constricting the flow of gas through the substrate, while the carbon black has a more effective pore structure.

The pressed LSFTa_32CB-substrate measured the highest degree of permeability with 11,5nPm and is considered the best structure with respect to viscous flow.

By assuming a pressure difference across the porous substrates, the flux of oxygen at room temperature can be calculated by Eq. 2.07. The flux of oxygen at operating temperature (800-1000 °C) can be estimated by including the change in gas viscosity as the temperature increases.

The calculated flux of oxygen at room temperature and an estimated flux at 1000 °C for the three porous substrates can be seen in appendix D2.

The best permeating structure was achieved by the LSFTA_32CB-substrate which achieves the highest permeability, Da. As tape casting is the envisioned fabrication process for the porous substrates, the substrates will be thinner than these pressed pellets, and the flux of oxygen will only increase with decreasing thickness.

As all produced substrates are showing sufficient flux of oxygen, the focus on the tape casting process and the substrate's mechanical strength becomes more distinguished. In the end, all substrate structures are well above the permeability requirements and will probably not limit the flux of a high end dense membrane. Mechanical characterization is needed to decide which of the substrates are the most promising.

5.6 Tape casting of porous substrates

The tape casted substrates sintered at 1275 °C were very fragile due to a low degree of sintering and were not further tested. A sintering temperature of 1350 °C was therefore set for the remaining substrates. The SEM-images in Figure 4-8 of the sintered substrate show good connected porosity for gas permeability, and the final thickness of the substrates was measured to 340-390µm.

Tape cast with the addition of fine LSFTa is showing a finer dispersion of pores, and with less completely dense areas compared to the same substrate without the fine particles. The same effect can be observed in the pressed substrates. This might indicate that the addition of fine particles led to a finer dispersion of pore former.

Tape cast of coarse LSFTa and cellulose acetate resulted in an inhomogenous tape. This is assumed to be due to poor mixing during slurry processing. TGA was set to tailor the sintering program and the substrates were sintered at 1350 °C according to the heat program in Figure 4-16.

All substrates with cellulose acetate seemed to warp in a specific direction according during the sintering program. The direction was related to its orientation when dried in the tape casting process.

The SEM-images of the cellulose acetate substrate in Figure 4-20 shows the inhomogeneous structure with an almost dense bottom layer, and a more porous top layer. The dense bottom layer was the side pointing down during drying and the porous layer was pointing up. This indicates that the pore former was indeed the cellulose acetate particles which could be observed on top of the tape cast, as this is where the pores are formed. The poor stabilization of pore former is therefore assumed to be the cause of the warping.

Stabilization of the cellulose acetate might be achieved by adjusting pH or by dispersing in a suitable solvent before the homogenization of the slurry. This was not attempted during this thesis due to time limitation.

5.7 Strength of tape casted substrates

Fracture load was recorded for the two successfully sintered tape casted substrates. A calculated biaxial strength of 37,4 and 34,2MPa was found for the LSFTa_32CB- and the LSFTa_32CB_20SA-substrate respectively.

Mechanical testing of ceramics is often performed on large quantities, as test values tend to scatter and fail by the weakest link theory [34]. Therefore, these results are not an accurate strength measurement of these materials. However, the measurements are considered representative by indicating that the substrates are within the desired strength range.

A strengthening effect from the added fine particles was expected as the apparent porosity of these substrates was lower than the ones without fine particles. The intention of adding fine particles was to achieve a strong structure by an increased degree of densification between the coarse particles.

From the SEM-images of the two carbon black substrates in Figure 4-17 and Figure 4-18, it appears that also a different effect is obtained. The structure of the substrate added fine particles have a finer structure which actually seems less dense compared to that of the substrate without fine particle. The two tested substrates achieved quite similar strengths, and whether or not the fine particles have might have a strengthening effect is difficult to prove without substantial testing.

The ball-on-ring test is sensitive to surface irregularities and performing accurate measurements on porous supports can be challenging. It might therefore be better to measure biaxial strength of porous substrates with a dense membrane sintered on top. Comparing the biaxial strength of the asymmetric membrane and of the dense membrane might give a good indication of the strength contribution from the porous substrate.

The previously achieved biaxial strength of similar was reported to 34MPa, and both tape casted substrates appear to be matching that strength.

5.8 Permeability of tape casted substrates

The permeability of the tape casted LSFTa_32CB was low compared to the pressed substrate of the same composition. The low permeability means that the tape casted structure is less suited than the pressed structure with respect to air flow, and if the two substrates were to be of the same thickness, the tape casted substrate would have the lower oxygen flux.

A lowered permeability was not expected from the tape casted substrates. The pressed substrates usually have a degree of horizontally orientated pores as a result from the uniaxial pressure forming the substrate. However, as vertical pore formation is the optimal formation with respect to gas flow, the horizontal orientation in the pressed substrates is assumed to be a drawback. Avoiding horizontally orientated pores should not be a problem for tape casted substrates, assuming stabilized slurry is obtained.

The tape casted substrate also obtained a higher porosity than the pressed substrates, which is assumed to be a result of the increased additive content used in the slurry. As the tape casted substrates achieves a higher porosity and avoids the formation of horizontal pores, the permeability was expected to be higher than the pressed pellets.

The lowered permeation must therefore be a result of the pore geometry in the tape casted substrate. As the tape casted substrate achieves a higher porosity, the pore geometry is clearly not favoring gas permeability.

The pore geometry in the tape casted substrate is naturally linked to the treatment of the pore former during green body processing. As the elongated shape of carbon black makes it very sensitive to impacts during processing, it might be that the morphology of the carbon black have varied in the two different processing methods used in this work. A change in pore former morphology will have a large effect on pore geometry, as can be seen by simply comparing the carbon black and cellulose acetate substrates. Therefore, if the carbon black

was crushed to fine powder during ball mill, leading to fine pore geometry, it might have lowered the gas permeation of the structure by not favoring viscous flow to the same extent as the pressed substrates.

Still, as the flux of oxygen passing through a substrate is dependant of substrate thickness according to Eq.2.07, the tape casted substrate still achieves a very high flux of oxygen. With a thickness of 391µm, the tape casted LSFTa_32CB achieved an average estimated flux of 115 ml min^{-1} cm^{-2} at 1000 °C (10mbar), which is more than an order above what is set for it to be commercially attractive.

These estimates are calculated by assuming a pressure difference of 10mbar across the substrate, which is presumed to be a modest assumption. Any increase in pressure difference will most likely only increase the flux of oxygen, according to Eq. 2.07.

The first and foremost motivation for adding a porous substrate to the dense membrane is to increase the strength of the final asymmetric membrane. According to these flux estimates, the porous substrates will probably not limit the flux of oxygen through any dense membrane. The thickness of the porous substrate can therefore be increased substantially, and thereby increasing its strength contribution, while still not be limiting to the flux of oxygen through the dense membrane.

By Eq.2.07 it follows that the tape casted LSFTa_32CB requires a pressure difference across the substrate of only 0,9mbar, or it can have its thickness increased to 3,4mm and still maintain a flux of 10 ml min^{-1} cm^{-2}. This is believed to be a low pressure requirement and a high thickness, and indicates that the permeability of the porous substrate is more than good enough to support a high end dense membrane in operation.

6 Conclusion

Coarse LSFTa was successfully synthesized by solid state reaction at 1300 °C. The powder has a main constituent particle size around 10µm with particles ranging up to 100µm. An optimum amount of dispersant (Darvan-C) was found to be 0,2 wt%, corresponding to a value of 27mg/m^2.

Pressed porous substrates were successfully sintered at 1350 °C, with carbon black and cellulose acetate acting as pore formers. All substrates were mainly made of very coarse LSFTa and the large particles seem to improve the degree of connected porosity in the substrate, and thereby increasing the viscous flow of gas.

Porous substrates made with carbon black shows the most promising pore formation with respect to air permeability, as it obtains high permeability from low porosity, compared to the substrates made with cellulose acetate pore former.

Tape casted porous $La_{0.2}Sr_{0.8}Fe_{0.8}Ta_{0.2}O_{3-\delta}$-substrates with carbon black pore former were successfully sintered at 1350 °C, with a final thickness of 391µm. Biaxial strength of tape casted porous substrates were measured and found to be 34-38MPa.

With 27 % apparent porosity the tape casted $La_{0.2}Sr_{0.8}Fe_{0.8}Ta_{0.2}O_{3-\delta}$-substrates achieved an average air permeability of 3,5nPm at room temperatures, which estimates to a flux of oxygen of 115 ml min^{-1} cm^{-2} at 1000 °C.

The estimated flux indicates that the porous substrates are able to support a high end membrane at operating temperatures, with respect to air permeability.

7 Further work

As the permeability achieved by the porous substrates is high above their criteria for them to be commercially attractive, the focus is shifted to its strength contribution. A substantial amount of mechanical testing is needed to get accurate fracture strengths, as this work only indicates what range of strength they are in. When the mechanical properties are properly specified, their geometry can be tailored according to their specific service.

However, the pressed substrates indicate that the flux can still be substantially increased. An increase in flux can also be one way of increasing the substrates strength contribution, as an improved permeating structure makes it possible to increase the thickness of the substrate while still maintaining a high flux of oxygen.

Optimization of the tape casting process might improve the permeability of the tape casted substrate to the level of which the pressed substrates are, and probably even further, as the horizontal pore formation can be avoided by tape casting. This can be achieved by using a more robust pore former, i.e. cellulose acetate, which is not as sensitive to impacts as the carbon black.

References

1. Bouwmeester, H.J.M., *Dense ceramic membranes for methane conversion.* Catalysis Today, 2003. 82(1-4): p. 141-150.
2. Bouwmeester, H. and A. Burggraaf, *Dense Ceramic Membranes for Oxygen Separation*, in *Handbook of Solid State Electrochemistry*1997, CRC Press.
3. Ni, M., M.K.H. Leung, and D.Y.C. Leung, *Technological development of hydrogen production by solid oxide electrolyzer cell (SOEC).* International Journal of Hydrogen Energy, 2008. 33(9): p. 2337-2354.
4. Gurauskis, J., et al., *Processing of thin film ceramic membranes for oxygen separation.* Journal of the European Ceramic Society, 2012. 32(3): p. 649-655.
5. Gurauskis, J., Ø.F. Lohne, and K. Wiik, *La0.2Sr0.8Fe0.8Ta0.2O3 − δ based thin film membranes with surface modification for oxygen production.* Solid State Ionics, (0).
6. Beuscher, U. and C. H. Gooding, *The influence of the porous support layer of composite membranes on the separation of binary gas mixtures.* Journal of Membrane Science, 1999. 152(1): p. 99-116.
7. Beuscher, U. and C.H. Gooding, *Characterization of the porous support layer of composite gas permeation membranes.* Journal of Membrane Science, 1997. 132(2): p. 213-227.
8. Chen, W., C.S. Chen, and L. Winnubst, *Ta-doped SrCo0.8Fe0.2O3-δ membranes: Phase stability and oxygen permeation in CO2 atmosphere.* Solid State Ionics, 2011. 196(1): p. 30-33.
9. Kreuer, K.D., *On the development of proton conducting materials for technological applications.* Solid State Ionics, 1997. 97(1-4): p. 1-15.
10. Kaus, I., et al., *Oxygen transport properties in La1-xSrxFe1-yMyO3-δ (M = Cr, Ti), 0.2 < x < 0.8, 0.2 < yTi < 0.5, 0.1 < yCr < 0.3.* Solid State Ionics, 2007. 178(11-12): p. 817-826.
11. Lein, H.L., et al., *Asymmetric proton conducting oxide membranes and fuel cells prepared by aqueous tape casting.* Solid State Ionics, 2008. 179(21-26): p. 1146-1150.
12. Weirich, M., *Characterisation of porous La6-xWO12-∂ supports*, 2011, NTNU Trondheim.
13. Wibe, P., *Optimisation of La0.2Sr0.8Fe0.8Ta0.2O3-δ for producing tape casted porous substrates*, 2011, Department of Materials Science and Engineering, NTNU.
14. Williams, M.V., et al., *Characterization of Gas Diffusion Layers for PEMFC.* Journal of The Electrochemical Society, 2004. 151(8): p. A1173-A1180.
15. Mizusaki, J., et al., *Nonstoichiometry and defect structure of the perovskite-type oxides La1−xSrxFeO3−°.* Journal of Solid State Chemistry, 1985. 58(2): p. 257-266.
16. Patrakeev, M.V., et al., *Electron/hole and ion transport in La1−xSrxFeO3−δ.* Journal of Solid State Chemistry, 2003. 172(1): p. 219-231.
17. Lohne, Ø.F., et al., *Effect of B-site substitution on the stability of La0.2Sr0.8Fe0.8B0.2O3−δ, B;= Al, Ga, Cr, Ti, Ta, Nb.* Solid State Ionics, (0).
18. Diethelm, S., et al., *Improved stability of La0.5Sr0.5FeO3 by Ta-doping for oxygen separation membrane application.* Solid State Ionics, 2009. 180(11–13): p. 857-860.

19. Ikeguchi, M., et al., *Improving oxygen permeability in SrFeCo0.5Ox asymmetric membranes by modifying support-layer porous structure.* Materials Letters, 2005. 59(11): p. 1356-1360.
20. Androff, N.W., L.F. Francis, and B.V. Velamakanni, *Macroporous ceramics from ceramic-polymer dispersion methods.* AIChE Journal, 1997. 43(S11): p. 2878-2888.
21. Weirich, M., et al., *Preparation of lanthanum tungstate membranes by tape casting technique.* International Journal of Hydrogen Energy, 2012. 37(9): p. 8056-8061.
22. Sanson, A., P. Pinasco, and E. Roncari, *Influence of pore formers on slurry composition and microstructure of tape cast supporting anodes for SOFCs.* Journal of the European Ceramic Society, 2008. 28(6): p. 1221-1226.
23. Beuscher, U. and C. H. Gooding, *The permeation of binary gas mixtures through support structures of composite membranes.* Journal of Membrane Science, 1998. 150(1): p. 57-73.
24. R&D Carbon Ltd, S., Switzerland, *RDC 145. Air Permeability*, 1989.
25. Kadoya, K., N. Matsunaga, and A. Nagashima, *Viscosity and thermal conductivity of dry air in the gaseous phase*1985: American Chemical Society and the American Institute of Physics for the National Bureau of Standards.
26. Rahaman, M.N., *Ceramic processing*2007, Boca Raton, Fla.: CRC/Taylor & Francis. 473 s.
27. Hotza, D. and P. Greil, *Review: aqueous tape casting of ceramic powders.* Materials Science and Engineering: A, 1995. 202(1–2): p. 206-217.
28. Huisman, W., T. Graule, and L.J. Gauckler, *Centrifugal slip casting of zirconia (TZP).* Journal of the European Ceramic Society, 1994. 13(1): p. 33-39.
29. Shojai, F., et al., *Electrostatic and electrosteric stabilization of aqueous slips of 3Y–ZrO2 powder.* Journal of the European Ceramic Society, 2000. 20(3): p. 277-283.
30. Briscoe, B.J., A.U. Khan, and P.F. Luckham, *Optimising the dispersion on an alumina suspension using commercial polyvalent electrolyte dispersants.* Journal of the European Ceramic Society, 1998. 18(14): p. 2141-2147.
31. Börger, A., P. Supancic, and R. Danzer, *The ball on three balls test for strength testing of brittle discs: stress distribution in the disc.* Journal of the European Ceramic Society, 2002. 22(9–10): p. 1425-1436.
32. Lipinska-Chwalek, M., et al., *Mechanical characterization of porous Ba0.5Sr0.5Co0.8Fe0.2O3−d.* Journal of the European Ceramic Society, 2011. 31(15): p. 2997-3002.
33. Wibe, P., *Development of ceramic membranes with composition La0.2Sr0.8Fe0.8Ta0.2O3-δ by means of tape casting II: Optimizing substrate with respect to porosity and structure*, 2011, Department of Materials Science and Engineering, NTNU.
34. De Smet, B., et al., *Weakest-link failure predictions for ceramics III: Uniaxial and biaxial bend tests on alumina.* Journal of the European Ceramic Society, 1992. 10(2): p. 101-107.

Appendix A – Standardizing $SrCO_3$

The result from thermal gravimetric analysis (TGA) of $SrCO_3$ is shown in Figure A-1.

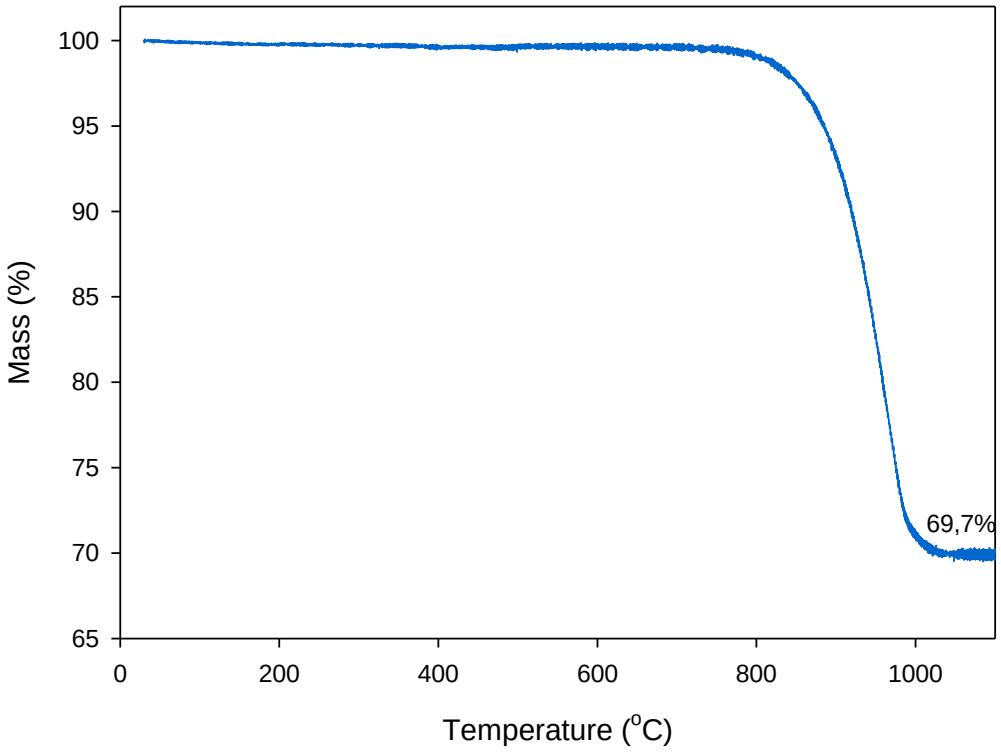

Figure A-1: Thermal gravimetric analysis of $SrCO_3$ for standardizing

Mass lost during heating was 30.3 %. Theoretical loss in mass is

$$1 - \left(\frac{MwSrO}{MwSrCO_3}\right) = 1 - \left(\frac{103{,}62 g/mol}{147{,}63 g/mol}\right) = 29.9\ \%$$

Concluding $SrCO_3$ was of ≈99,4 % purity, assuming all impurities were removed during heating.

Appendix B1 – Synthesis of $La_{0.2}Sr_{0.8}Fe_{0.8}Ta_{0.2}O_{3-\delta}$ by spray pyrolysis

$La_{0.2}Sr_{0.8}Fe_{0.8}Ta_{0.2}O_{3-\delta}$ was produced by PhD-student Ørjan F. Lohne using spray pyrolysis. Aqueous solutions of $Fe(NO_3)_3$, $Sr(NO_3)_2$ and La-EDTA complex and Ta-peroxo-citrato complex were mixed in correct stoichiometry, controlled by thermal gravimetric standardization and spray pyrolysed at 1000 °C with a feed rate of 10 L/h.

Synthesis of the aqueous tantalum and lanthanum solutions is given in the following flowcharts

Synthesis of Ta-peroxo-citrato complex

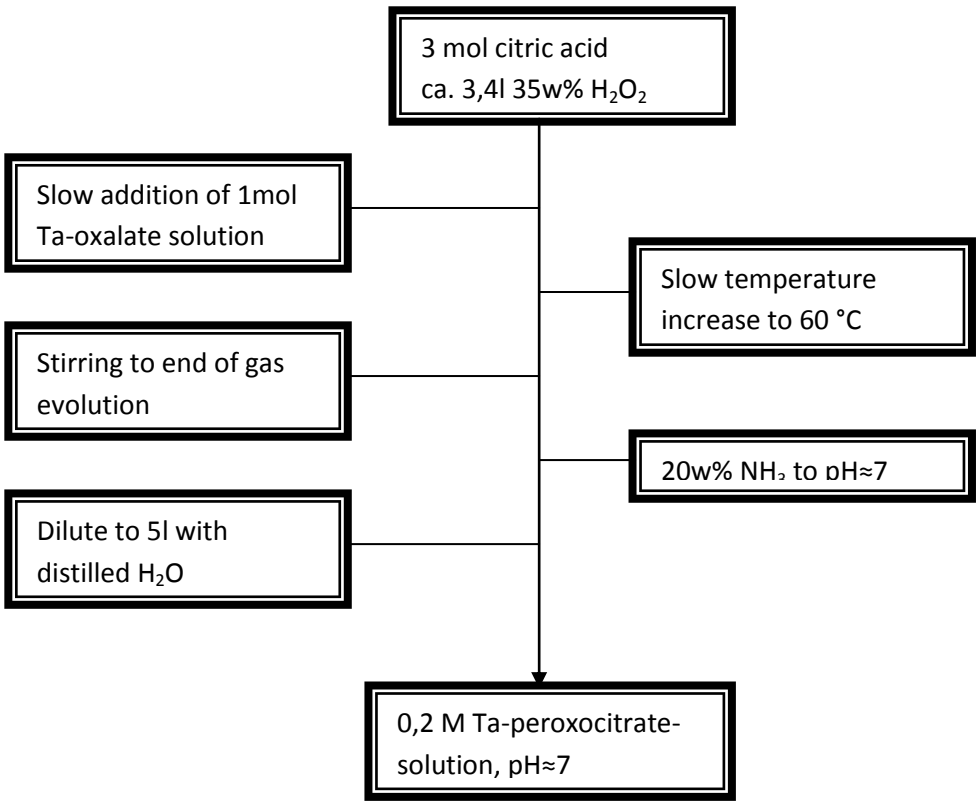

Appendix B2 - Synthesis of $La_{0.2}Sr_{0.8}Fe_{0.8}Ta_{0.2}O_{3-\delta}$ by spray pyrolysis

Synthesis of La-EDTA complex

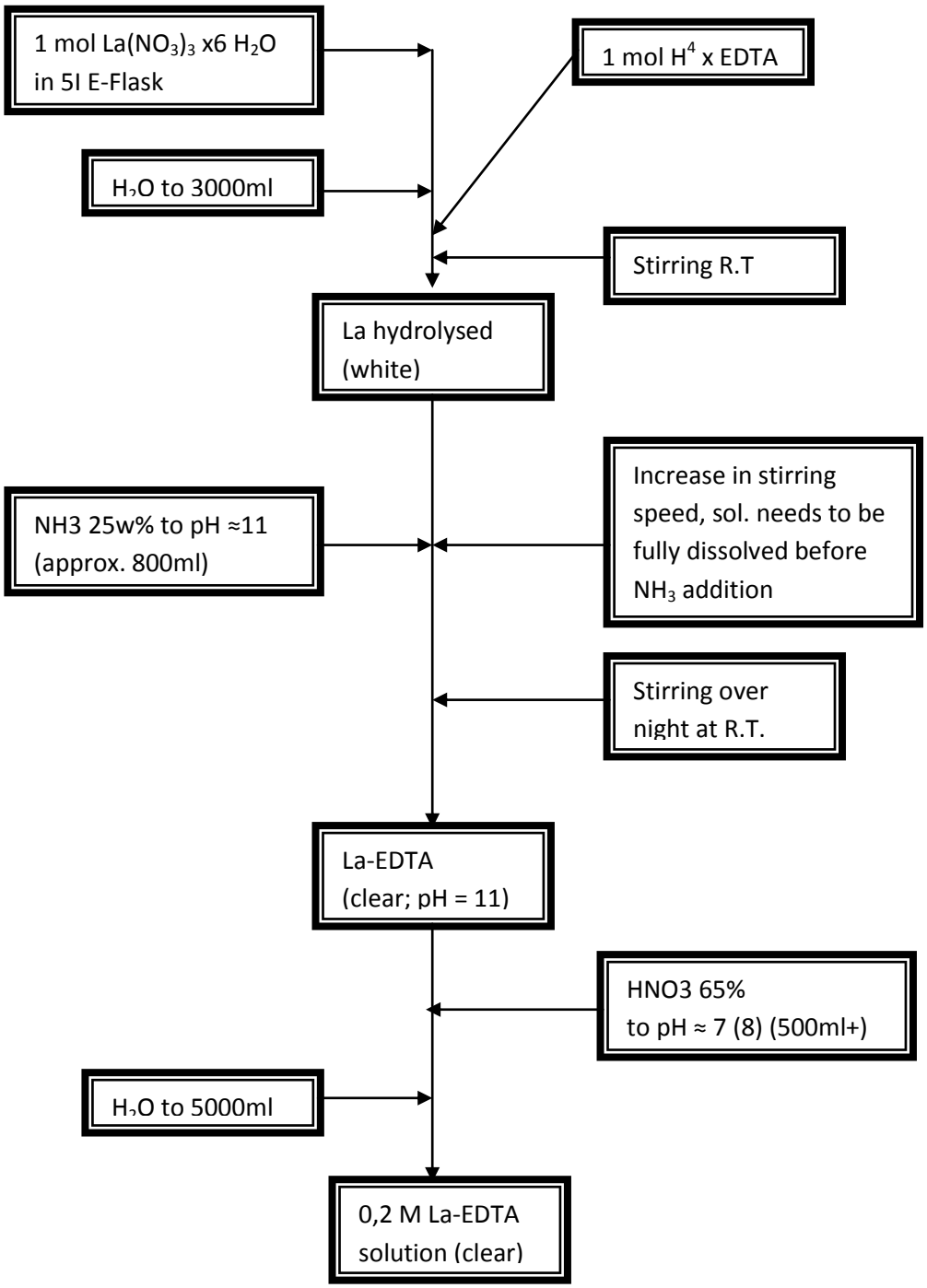

Appendix C1 – Coverage of coarse $La_{0.2}Sr_{0.8}Fe_{0.8}Ta_{0.2}O_{3-\delta}$ by fine $La_{0.2}Sr_{0.8}Fe_{0.8}Ta_{0.2}O_{3-\delta}$

	Coarse $La_{0.2}Sr_{0.8}Fe_{0.8}Ta_{0.2}O_{3-\delta}$	Fine $La_{0.2}Sr_{0.8}Fe_{0.8}Ta_{0.2}O_{3-\delta}$
BET-Sa	0.5368 m^2/g	11.3949 m^2/g

Mass, M, of fine powder needed to constitute a percentage of the surface area, Sa, formed by a given amount (5g in this case) of coarse powder can written as

$$M_{fine\ powder} = \frac{Sa(5g)_{coarse\ LSFTa} \cdot \%\ coverage}{Sa_{fine\ LSFTa}}$$

The mass of fine $La_{0.2}Sr_{0.8}Fe_{0.8}Ta_{0.2}O_{3-\delta}$ needed to form 5% of the surface area of 5g of coarse $La_{0.2}Sr_{0.8}Fe_{0.8}Ta_{0.2}O_{3-\delta}$ will therefore equal to

$$M_{fine\ powder} = \frac{0.5368\frac{m^2}{g} \cdot 5g \cdot 5\%\ coverage}{11.3949\frac{m^2}{g}} = 0.012g$$

The mass of fine $La_{0.2}Sr_{0.8}Fe_{0.8}Ta_{0.2}O_{3-\delta}$ needed to form 5, 10 and 20% of the surface area of 5g of coarse $La_{0.2}Sr_{0.8}Fe_{0.8}Ta_{0.2}O_{3-\delta}$ is shown in the table below.

Sample	Solid state powder (g)	Coverage (%)	Spray pyrolised powder (g)
#1	5	5	0.012
#2	5	10	0.024
#3	5	20	0.048

Appendix D1 – Permeability measurements

Three measurements of each sample were made. Average measurement was calculated and actual permeability was calculated from

$$D_{a\,(real)} = D_{a(1)} \cdot \frac{A_1}{h_1} \cdot \frac{h_2}{A_2}$$

	Measured permeability (nPm)	Averagemeasure (nPm)	Thickness, h_2 (m)	Actual permeability (nPm)
Sintered at 1275 °C				
LSFTa_32CB	14,260 - sample broke	14.26	$1.67 \cdot 10^{-3}$	29,8
LSFTa_32CB_20SA	8.933, 8.841, 8.954	8.909	$2.47 \cdot 10^{-3}$	27,5
LSFTa_32CA	5.115, 5.163, 5.180	5.153	$2.44 \cdot 10^{-3}$	15,7
Sintered at 1350 °C				
LSFTa_32CB	4.674, 4.700. 4.714	14.696	$1.96 \cdot 10^{-3}$	11,5
LSFTa_32CB_20SA	4.369, 4.357, 4.359	13.085	$1.52 \cdot 10^{-3}$	8,3
LSFTa_32CA	5.633, 5.662, 5.666	5.654	$1.29 \cdot 10^{-3}$	9,1
Tape casted substrate				
LSFTa_32CB	7.946, 7.841, 7.830	7.872	$0.297 \cdot 10^{-3}$	2.93
LSFTa_32CB	7.604, 7.435, 7.413	7.484	$0.304 \cdot 10^{-3}$	2.84
LSFTa_32CB	8.144, 8.023, 8.023	8.063	$0.344 \cdot 10^{-3}$	3.46

So for the LSFTa_32CB-substrate sintered at 1275 °C the actual permeability can be calculated from

$$D_{a\,(real)} = 14{,}260nPm \cdot \frac{\pi(0.025m)^2}{0.02m} \cdot \frac{1{,}67 \cdot 10^{-3}m}{\pi(0.005m)^2} = 29{,}8nPm$$

Appendix D2 – High temperature flux

By assuming a Δp of 10mbar across the porous substrates, the flux of oxygen can be calculated by

$$\frac{V}{t} = \frac{D \cdot A \cdot \Delta p}{h \cdot \eta}$$

Table 0-1: Calculated flux of oxygen at 1000 °C for porous substrates

Substrate sample	Oxygen flux (ml min^{-1} cm^{-2})
Temperature	*1000 °C*
Coarse LSFTa and 32 vol% Carbon black	69,3
Coarse LSFTa and 32 vol% Carbon black w/ fine LSFTa sintering aid	64,5
Coarse LSFTa and 32 vol% Cellulose acetate	83,3

The estimated flux of oxygen from 0-1000 °C for the three pressed substrates and the tape casted LSFTa_32CB sintered at 1350 °C is plotted in Figure A-.

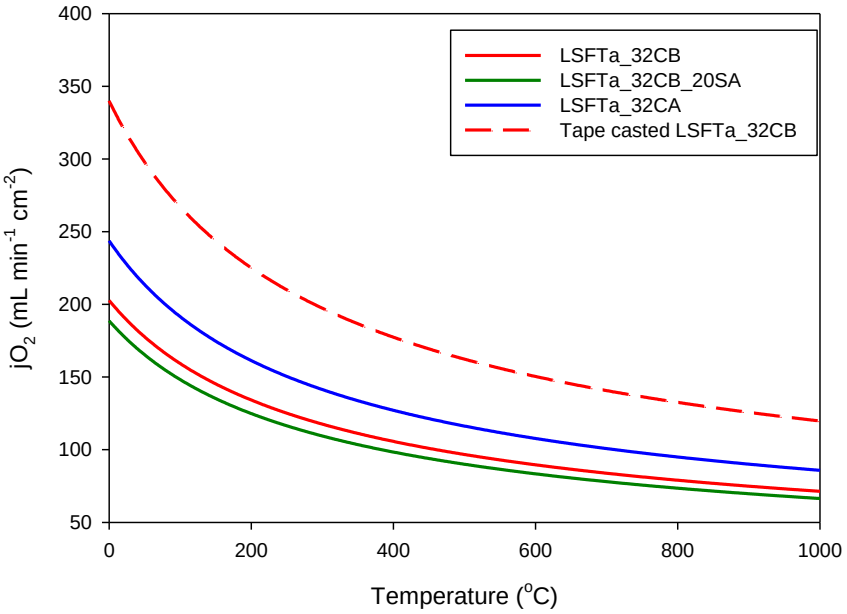

Figure A-2: Estimated oxygen flux at elevated temperatures of porous substrates sintered at 1350 °C

Appendix E – Ash contents of pore formers

Table 0-1: Weight measurement of crucibles before heating, amount of pore former added in crucibles and weight measurement of crucibles after heating to 800 °C

Carbon black, sample #	1	2	Cellulose acetate, sample #	1	2
Crucible weight before, M_1	12.060g	42.257g	Crucible weight before, M_1	11.513g	11.241g
Carbon black added	0.663g	1.562g	Cellulose acetate added	0.824g	1.069g
Crucible weight after, M_2	12.065g	42.268g	Crucible weight after, M_2	11.513g	11.241g

Ash contents can easily be calculated from fraction of mass remaining after heating to

$$Ash\ content = \frac{(M_{2\ crucible} - M_{1\ crucible})}{M_{Pore\ former}}$$

Resulting in an approximate ash contents of ≈0.73% for carbon black compared to a low <0.1% for cellulose acetate.